Cancer immunotherapy responses persist after lymph node resection

Hengbo Zhou[1,2], James W. Baish[3], Meghan J. O'Melia[1], Laurel B. Darragh[4], Emma Specht[5], Juliane Czapla[5], Pin-ji Lei[1], Lutz Menzel[1], Johanna J. Rajotte[1], Mohammad R. Nikmaneshi[1], Mohammad S. Razavi[1], Matthew G. Vander Heiden[2,6], Jessalyn M. Ubellacker[7], Lance L. Munn[1], Genevieve M. Boland[5], Sonia Cohen[5], Sana D. Karam[4] and Timothy P. Padera[1]

1. Edwin Steele Laboratories, Department of Radiation Oncology, Massachusetts General Hospital

2. Koch Institute for Cancer Research and Department of Biology, Massachusetts Institute of Technology

3. Department of Biomedical Engineering, Bucknell University

4. Department of Radiation Oncology, University of Colorado Anschutz Medical Campus

5. Department of Surgery, Massachusetts General Hospital

6. Department of Medical Oncology, Dana-Farber Cancer Institute

7. Department of Molecular Metabolism, Harvard T.H. Chan School of Public Health

Abstract:

Due to the critical role of lymph nodes (LNs) in the initiation and maintenance of adaptive immune responses, it is unclear whether surgical removal or ablative radiation therapy of LNs should be performed in patients with metastatic LNs that will receive immunotherapy. Surgical removal of LNs to prevent metastatic recurrence, including sentinel lymph node biopsy (SLNB) and completion lymph node dissection (CLND), are performed in routine practice. However, removing LNs eliminates opportunities for generating anti-cancer immune responses that are enhanced with immune checkpoint blockade (ICB). Balancing the potential risks and benefits of LN surgery is necessary to maximize outcomes for patients. In contrast to mouse studies using ectopic tumor implantation[1,2], the phase III clinical trial NCT00636168 found patients with completely resected stage III melanoma (primary tumor, sentinel LNs and disease-related LNs all removed) still benefited from anti-CTLA4 inhibition. Our retrospective analysis demonstrated that stage III melanoma patients with SLNB or CLND have similar response to anti-PD1 inhibition. Using orthotopic murine mammary carcinoma and melanoma that have spontaneous LN metastases, we show that responses to ICB persist in mice after resection of TDLNs. Mechanistically, after disruption of normal lymphatic drainage, antigen can access adjacent lymphatic basins (lymphosomes) and be transported to distant LNs, which extends the responsiveness to ICB. By evaluating head and neck cancer patients treated by neoadjuvant durvalumab and irradiation, we show that distant LNs remain reactive in the absence of metastatic disease in ICB responder patients after tumor and disease related-LN resection, indicating anti-cancer immune reactions occur in distant LNs after TDLN removal in patients. Additionally, after TDLN dissection in mouse models, ICB delivered to distant LNs generated greater survival benefit, compared to systemic administration. In complete responders, anti-tumor immune memory induced by ICB was systemic rather than confined within lymphoid organs. Based on these findings, we constructed a computational model to predict free antigen trafficking in patients that will undergo LN dissection. Collectively, we propose that ICB efficacy persists in tumors of the trunk and extremities after removing original TDLNs because antigen can be transported through interstitial tissues to adjacent lymphosomes to gain access to alternative LNs, where anti-cancer immune responses can be generated and maintained.

Introduction:

Recent advances in understanding of the mechanisms of T cell activation and exhaustion led to the identification of several immune checkpoints, such as programmed death 1 (PD-1)[3,4] and cytotoxic T lymphocytes antigen 4 (CTLA-4)[5,6], which have been used as therapeutic targets[7,8]. Immune checkpoint blockade (ICB) has been approved to treat many cancers including

melanoma[9,10], non-small cell lung cancer[11,12], renal cell carcinoma[13], Hodgkin lymphoma[14], hepatocellular carcinoma[15,16], and gastric carcinoma[17]. However, an improved understanding of ICB mechanisms *in vivo* is necessary for immunotherapy to benefit more patients.

Lymph nodes (LNs) are secondary lymphoid organs that surveil tissue fluids and initiate adaptive immunity[18]. Due to the direct drainage of interstitial fluid from tumor tissue in the lymphatic basin (lymphosome), metastatic dissemination to tumor-draining lymph nodes (TDLNs) occurs in the early stage of cancer growth[19]. Colonization in LNs can block nodal entry of naïve lymphocytes[20], expand regulatory T cells (Tregs)[21,22] and induce systemic tolerance to favor distant metastasis of cancer cells[22]. LN metastases can also further disseminate to additional metastatic sites[23,24]. Therefore, LN metastatic burden is a strong prognostic factor for patient outcome. Sentinel lymph node biopsy (SLNB) and completion lymph node dissection (CLND) are commonly performed[25-29] to help stage disease and reduce disease burden. However, in an era of effective systemic therapies, the morbidity of these surgical LN procedures and the controversy regarding their role in preventing recurrence/metastatic disease in certain cancers, including early-stage breast cancer[30], ovarian cancer[31], cervical cancer[32], and melanoma[33], has shifted clinical practice toward less aggressive LN surgery for the initial management of microscopic metastatic disease.

Recent work has demonstrated that tumor-specific T cells and non-exhausted tumor-specific memory cells are enriched in TDLNs, but not in non-TDLNs[34,35]. In addition, PD-1/PD-L1 interaction between conventional dendritic cells (DCs) (PD-L1+) and tumor-specific T cells (PD-1+) is abundant in TDLNs[34]. Intrapleural delivery of low-dose PD-L1 antibody to TDLNs can induce anti-tumor immunity against AC29 tumors (mesothelioma)[34]. Additional studies, using B16F10 (melanoma), 4T1 (mammary carcinoma) and E0771(mammary carcinoma) tumors, found selective administration of ICB to TDLNs can improve ICB potency, compared to systemic administration[36,37]. These data suggest that removal of TDLNs could potentially impair ICB outcome. Indeed, anti-PD-1 or anti-4-1BB efficacy can be abolished by TDLN dissection in MC38 (colon adenocarcinoma) or CT26 (colon carcinoma) tumors ectopically grafted in the skin[1,2]. Similarly, responses can be ablated by TDLN lymphadenectomy at any point during anti-PD-L1 treatment in subcutaneously grafted B16F10 (melanoma) tumors expressing lymphocytic choriomeningitis virus glycoprotein[35]. However, in the phase III clinical trial NCT00636168, completely resected stage III melanoma patients, from whom sentinel LNs and metastatic LNs were removed, still responded and benefited from ipilimumab (targeting CTLA-4), indicating that persistent presence of TDLNs may not be required for ICB efficacy[38]. Further, in the phase I trial NCT04274816, lymphatic basin administration of tremelimumab (targeting CTLA4) after tumor resection led to a systemic reduction of Tregs and activation of effector T cells. This response persisted up to 3 months after subsequent SLNB, suggesting that the ICB-mediated immune response was not confined only within sentinel LNs[39]. Due to the important role of LNs in the adaptive immune response, it is imperative to evaluate the effects of SLNB and CLND on ICB efficacy.

Here, through retrospective analysis, we found that regardless of the extent of LN surgery, stage III melanoma patients benefited similarly from adjuvant anti-PD1 inhibition. By using orthotopic breast cancer and melanoma models in mice, we demonstrated that neither SLNB nor CLND eliminates ICB efficacy, despite the purported important role of TDLNs in anti-tumor responses. Mechanistically, after TDLN dissection, antigen can be transported to distant LNs through redirected lymph drainage, which contributes to the residual responsiveness to ICB. This phenomenon is corroborated in head and neck cancer patients—treated by neoadjuvant durvalumab and irradiation therapy followed by adjuvant durvalumab—by the presence of reactive distant LNs after primary tumor resection and LN dissection. Thus, consistent with clinical observations, ICB efficacy is not reliant solely on the presence of the original TDLNs, and ICB can be effective against locoregional recurrence even after TDLN dissection.

Results:

100 **The extent of lymph node surgery does not impact melanoma response to ICB clinically**

101 Prior to the availability of effective systemic therapies for patients with melanoma, LN surgery
102 played a major role in the treatment of patients with locoregional disease. Any patient with
103 clinically evident LN metastases or a positive SLNB underwent CLND for disease control. In
104 2017 MSLT-II[33], a randomized trial of CLND vs observation in patients with positive SLNB,
105 demonstrated that CLND provided no melanoma-specific survival (MSS) benefit to patients with
106 melanoma identified within the SLN. Given the morbidity of CLND, this trial changed clinical
107 practice to favor observation after a positive SLNB, with CLND reserved for clinical disease
108 recurrence in the draining LN basin. Approximately 20% of patients would ultimately recur in
109 the draining nodal basin, sparing 80% of patients with a positive SLNB from the unnecessary
110 morbidity of CLND[33].

111 The MSLT-II trial reflected the era of melanoma treatment prior to the introduction of ICB. With
112 the approval of effective systemic therapies, the role of LN surgery—other than for staging—has
113 been called into question. Given the importance of TDLNs for ICB response in mouse
114 models[1,2,35], we asked whether the extent of LN surgery would impact the effectiveness of ICB
115 treatment. To assess this, we analyzed a cohort of 66 patients who underwent surgery for stage
116 III melanoma followed by adjuvant treatment with at least one line of anti-PD1 therapy
117 (nivolumab or pembrolizumab) at Massachusetts General Hospital. Within this adjuvant ICB
118 cohort, 50 patients underwent SLNB alone while 16 patients underwent CLND. There was no
119 statistically significant difference in MSS (**Figure 1 A**) or recurrence-free survival (RFS)
120 (**Figure 1 B**) between patients who underwent SLNB alone versus those who underwent CLND.
121 After further stratification, no difference was detected in local (**Figure 1 C**) or distant (**Figure 1**
122 **D**) RFS either. These data demonstrate that patients who have undergone LN surgery still benefit
123 from ICB treatment, and that the extent of LN surgery within the draining lymph node basin does
124 not impact outcomes in the setting of ICB.

125 **ICB response persists after TDLN dissection in mice**

126 To experimentally test the impact of TDLN dissection on ICB efficacy in murine models, we
127 used orthotopic, syngeneic mouse melanoma (B16F10) and mammary carcinoma (E0771)
128 models. SLNB was modeled by removing the inguinal (IN) LN in C57BL6 mice, which drains
129 the upper hindleg and 4th mammary fat pad of mice. Of note, as surgery can cause multiple
130 effects in cancer patients, including the potential for causing metastatic spread after primary
131 tumor removal and trauma-induced immunosuppression[40,41], sham LN removal surgery was
132 performed on all animals in control groups. After 10 days of recovery, B16F10 or E0771 cells
133 were introduced to the dermis on the lower flank or 4th mammary fat pad, respectively. 7 days
134 later, 3 doses of PD-1 blocking antibody (10mg/kg) were administered intraperitoneally (every 2
135 days for B16F10 tumors or every 3 days for E0771 tumors). Compared to IgG control treated
136 mice, PD-1 inhibition increased overall survival in both the sham and SLN removed (SLNB)
137 mice. Interestingly, in groups treated with anti-PD-1, there was no difference in overall survival
138 between the sham surgery mice and the SLNB counterparts (**Figure 2A**). To mimic CLND, a
139 radical procedure that is increasingly less common in the clinic[30-33], ipsilateral IN, axillary (AX),
140 and brachial (BR) LNs were surgically removed, as each is in the region can receive lymphatic
141 drainage from the tumor site[2,42]. Similar to SLNB, there was residual ICB response after CLND,
142 and no statistically significant difference in overall survival was found between sham and CLND
143 conditions when animals were treated with PD-1 blocking antibody (**Figure 2B**).

144 Next, we measured whether anti-tumor immunity is retained solely in TDLNs after tumor
145 establishment. Thus, we tested the effects of SLNB and CLND after primary tumor implantation.
146 B16F10 or E0771 cells were orthotopically implanted 6 days prior to surgery. Sham, SLNB or
147 CLND was performed at day 6 and 3 doses of anti-PD-1 treatment was initiated at day 7 (every 2
148 days for B16F10 tumors or every 3 days for E0771 tumors). Similar to pre-emptive surgery,
149 neither SLNB nor CLND significantly affected overall survival in anti-PD-1 treated mice
150 compared to sham surgery (**Figure 2C**). Although there was no significant decrease in survival

151 after LN surgery, fewer mice remained tumor-free in the LN dissection conditions (**Figure 2D)**.
152 These findings are not consistent with recent investigations using MC38 and CT26 tumor models
153 grown ectopically in the subcutaneous setting[1,2]. To determine whether implantation site can
154 affect ICB outcome, E0771 cells were introduced to the dermis and LN dissection was conducted
155 either pre-emptively or after tumor establishment. Intriguingly, aggressive CLND can impair
156 anti-PD-1 efficacy in the ectopic setting (**Supp Figure 1 A&B**), indicating altered immune
157 response can occur when tumor cells are introduced to an ectopic site.

158 **Other LNs are required for ICB response after TDLN dissection**

159 Because of the surprising finding that neither SLNB nor CLND affects the overall survival
160 benefit of ICB treatment in mice, we sought to examine whether LNs in general are essential for
161 ICB response. To that end, lymphotoxin alpha (Lta) knock out (KO) mice —*Lta*^{tm1Dch} (C57bl/6
162 background), referred to throughout as *Lta* KO mice were used. These mice lack Peyer's patches
163 and multiple LNs including popliteal (PO), IN, BR and AX LNs, among other missing lymphoid
164 tissues[43]. Of note, the bone marrow is functional in these animals and the lack of LNs is likely
165 caused by development defects[43-45]. Although the splenic structure is disorganized by *Lta*
166 deletion, the number of lymphocytes, the composition of the types of lymphocytes and their
167 homing and effector abilities are normal in both the spleen and in peripheral blood[43-46]. B16F10
168 or E0771 cells were orthotopically implanted in *Lta KO* mice and 3 doses of PD-1 blocking
169 antibody were administered starting 7 days after tumor implantation (every 3 days). Strikingly,
170 compared to responses in wildtype (WT) mice (sham animal survival curves from SLNB study,
171 **Figure 2A**, were plotted for comparison), slowed tumor growth and improved survival from PD-
172 1 inhibition were abolished in these mice lacking LNs (**Figure 2E**), suggesting adaptive immune
173 responses generated in LNs contribute to ICB response. Further, these results suggest that LN-
174 dependent compensatory mechanisms occur after TDLN dissection to maintain anti-PD-1
175 responses in wild-type mice.

176 **LN dissection alters lymph drainage and promotes antigen access to distant lymphoid**
177 **organs**

178 To interrogate the mechanism by which animals that have undergone LN surgery generate ICB-
179 induced immune responses, we first measured the local transport of surrogate antigens to
180 alternative draining lymph nodes (DLNs) after SLNB or CLND. 2 million Dalton (MD) FITC-
181 dextran and 4.4 kilodalton (kD) TRITC-dextran were used as surrogate biomolecules with
182 different sizes. The dextran mixture was introduced to the 4th mammary fat pad in animals that
183 had undergone sham surgery or dissection of the IN LN (SLNB) or the IN/AX/BR LNs (CLND).
184 After 6 hours, ipsilateral IN, AX, BR LNs remaining in the relevant groups as well as all
185 contralateral IN LNs were collected for microscopic examination. In LNs, the majority of 2 MD
186 dextran was found to be aggregated in the subcapsular sinus (SCS) region—showing transport by
187 the lymphatic system—while 4.4kD dextran was sparsely distributed throughout the LN (**Figure**
188 **3A**). Based on these data, it is not clear whether the 4.4kD dextran arrived in the LN from the
189 lymph or the blood. Small biomolecules can enter LNs via the lymph or blood circulation[47].
190 However, our data show that the large biomolecules rely heavily on the lymphatic system to
191 arrive in the LN. Both types of dextran can be taken up by phagocytes resident in cortical,
192 paracortical and inter-follicular spaces (**Figure 3A**). 2 MD dextran abundance in AX LNs from
193 SLNB animals is comparable to counterparts in IN or AX LNs from sham animals (**Figure 3B**),
194 indicating resection of IN LN does not disrupt the drainage to the downstream AX LN.
195 Interestingly, 2 MD dextran was also detected entering the SCS of contralateral IN LNs in
196 certain animals (**Figure 3C**). Compared to sham animals, there was an increased incidence of 2
197 MD dextran drained to contralateral IN LNs of CLND animals (**Figure 3B**). Inconsistent with a
198 previous report[2], there was limited drainage from mammary fat pad to BR LNs across conditions,
199 suggesting BR LNs are not main DLNs (**Figure 3B**). Nonetheless, because BR LNs are in axilla
200 region, removing BR LN along with IN LN and AX LN is a relevant approach to model CLND
201 (basin dissection) which also removes non-DLNs[30,33]. Collectively, these data show that CLND

disrupts the normal patterns of lymph drainage, which results in lymph (and surrogate antigen) being transported to alternative LNs.

Next, we determined whether interstitial transport from a disrupted lymphosome could cross the body midline and enter adjacent lymphosomes. To that end, an incision was made to the midline skin (from lower abdomen to chest) in CLND mice, and 2MD dextran was injected to the ipsilateral 4th mammary fat pad. Strikingly, 2MD dextran transport to contralateral LNs was only detected in mice with intact midline skin, but not in mice with midline injury (**Figure 3D**). Thus, these data show that interstitial fluid with solutes can move across the midline through the dermis and reach an adjacent lymphosome draining to distant LNs after CLND. These results suggest that when primary LN(s) are removed, lymph can be driven to the next accessible lymphosome, even if the DLNs are anatomically distant (**Figure 3E**).

To further test whether—beyond the mammary fat pad region—antigen access to distant LNs can be enhanced when local lymphatic drainage is ablated, we performed sham surgery or ipsilateral popliteal (PO), IN, AX and BR LN dissection on mice (ILND condition). Subsequently, a mixture of 2MD and 4.4kD dextran was injected to the foot pad of those animals. Due to this anatomic site, injection-induced antigen convection to distant sites was minimized, and all LNs along the direct drainage path were absent. Similar to findings described in **Figure 3B**, we discovered that 6 hours after injection, 2MD dextran was mainly located in ipsilateral PO, IN and AX LNs when lymphatic drainage was intact, whereas ILND re-routed 2MD dextran transport to contralateral IN and AX LNs (**Supp Figure 2**). The lack of 2MD dextran in contralateral PO LNs suggests that, once taken up by lymphatic vessels of an adjacent lymphosome, the lymph still follows the normal drainage patterns, and does not undergo retrograde flow or circulate significantly through the blood in ILND mice (**Supp Figure 2**). In contrast, 4.4kD dextran, with its smaller size was found in all remaining LNs (**Supp Figure 2**), suggesting transport through the blood. The compensatory drainage phenomenon in the lower limb suggested by our data has also been reported clinically. A recent indocyanine green fluorescence lymphography study found that in patients with cancer treatment related lower limb lymphoedema, lower limb interstitial fluid can be transported across the lower abdomen to the contralateral inguinal region[48].

Collectively, our data show that lymph is drained to downstream LNs after SLNB, while CLND causes disruption of lymphatic vessel transport, which leads to a reliance on interstitial transport to carry the surrogate antigens to adjacent lymphosomes (drainage basins), where they are taken up by local lymphatics and transported to distant LNs. These findings are consistent with the clinical observation that breast cancer patients who have undergone AX LN dissections are more likely to develop altered lymph drainage to contralateral AX LNs[49]. Similarly, radiation therapy can cause lymphatic drainage aberration in breast cancer patients, which decreases flow to the ipsilateral axilla while increasing flow to contralateral axilla[50].

In addition to distant LNs, we found that 2MD dextran was also detectable in spleens from both sham and ILND mice. 2MD dextran was more abundant in spleens of mice in the ILND condition (**Figure 3F**). These large dextran molecules were mainly detected in the B cell follicles and adjacent marginal zone macrophages, instead of residing in macrophage-rich red pulp[51] (**Figure 3G**), indicating the potential for the generation of immune responses in the spleen against antigen arising from distal tissue, compensating for the loss of DLNs.

TDLN dissection stimulates immune responses in distant LNs

Since distant LNs of CLND mice can be exposed to interstitial fluid from the primary tumor site, we next examined whether tumor-specific immunity can be generated in these distant LNs. B16F10 cells expressing ovalbumin (257-264: SIINFEKL) were implanted to sham surgery or CLND mice and anti-PD-1 treatment started after 7 days. Subsequently, the spleen as well as any ipsi- and contra-lateral LNs were collected for immunofluorescence and flow cytometry analyses. CD8 T cell expansion was detected in ipsilateral LNs in sham surgery mice and

contralateral LNs in CLND mice (**Figure 4A**). Moreover, spleens in CLND animals contained an equal percentage of CD8 T cells compared to the sham surgery counterparts (**Figure 4B**), indicating that the immune reaction to the tumor was not confined within TDLNs. We also measured the abundance of SIINFEKL-specific CD8 T cells (referred to throughout as OVA-T cells) to assess tumor-specific immune responses (**Figure 4C**). Consistent with previous investigations[34,36], OVA-T cells were found to be predominantly enriched in sham surgery ipsilateral LNs, whereas certain CLND contralateral LNs, but not cervical LNs, also harbored high numbers of OVA-T cells (**Figure 4D**), indicating a directional spread of antigen consistent with adjacent lymphosomes, instead of systemic spread . Additionally, the abundance of OVA-T cells was comparable in spleens and blood of both sham and CLND mice (**Figure 4D**), demonstrating that the absence of TDLNs does not ablate circulating tumor-specific T cells.

To better recapitulate the clinical situation, ICB-induced tumor-specific T cell response was tested in an adjuvant setting. Two weeks after tumor implantation in intact mice, primary tumor removal was performed with or without CLND. After 3 days of recovery, mice were given anti-PD-1 treatment. No difference was found in OVA-T cell abundance between sham ipsilateral LNs and CLND contralateral LNs (**Figure 4E**), indicating, that even without the primary tumor antigen source, distant LNs can generate tumor-specific immune response after the removal of the initial TDLNs. To test whether tumor-specific T cells from distant LNs can infiltrate recurrent tumors, B16F10-OVA tumors were implanted into Kaede mice[52], and the tumors were resected with and without CLND; the mice were then treated with adjuvant anti-PD1 inhibition. After 14 days, these mice were implanted with B16F10-OVA tumors in the same primary site—to model recurrence—followed by photoconversion of contralateral IN LNs. Strikingly, Kaede red+ OVA-T cells were present in recurrent tumors, and the abundance was greater in CLND mice, compared to mice that did not undergo LN surgery (**Figure 4F**), suggesting that immune cells from distant LNs can be activated and traffic to recurrent tumors.

Antigen can disseminate by advection with interstitial fluid, but it can also be carried by antigen-presenting cells (APCs), which may access distant LNs after primary DLN resection. To assess the contribution of APCs, sham surgery or dissection of PO, IN, AX and BR LNs (ILND condition) was conducted in cohorts of mice. After recovery from surgery, bone marrow-derived DCs (BMDCs) from donor mice were loaded with OVA, stimulated with lipopolysaccharide (LPS) and subsequently injected in the foot pad of sham or ILND mice. Even though it has been demonstrated that BMDCs contain heterogeneous macrophage and DC populations[53], this model is able to test APC-mediated T cell priming in LNs. Intriguingly, we found that OVA-T cells were significantly enriched in ipsilateral LNs of sham mice and contralateral LNs of ILND mice, but not contralateral LNs of sham animals (**Figure 4G**). These results suggest that antigen carrying-APCs also have greater access to distant LNs when lymphatic drainage is disrupted.

As our data show that large dextran molecules are enriched in the spleen after CLND (**Figure 3 E&F**) and accompanied by CD8 T cell expansion (**Figure 4B**) and a tumor-specific T cell response (**Figure 4D**), we next determined whether the spleen is essential for residual ICB response in mice after CLND. To that end, sham surgery (SP+ condition) or splenectomy (SP- condition) was performed 2 weeks prior to CLND, and E0771 tumors were implanted and treated as described before. Unexpectedly, splenectomy did not significantly affect the overall survival in anti-PD-1 treated mice. Complete responders were less frequent, but still present, in SP- mice (**Supp Figure 3A)**. Further, all complete responders (5/5) from the SP+ condition and 2 out of 3 of SP- counterparts could completely reject tumor rechallenge, (**Supp Figure 3B)**. Altogether, these data suggest that the spleen contributes, but only marginally, to the ICB response and long-term immune memory formation in CLND mice.

Mathematical modeling of antigen access to adjacent lymphosomes via dermal interstitial transport after TDLN dissection

Because our data show that antigen can access adjacent lymphosomes and activate distant LNs (**Figure 3&4)**, we next used mathematical modeling to help understand this process from a

pharmacokinetic perspective. To that end, we developed a multi-scale computational model of transport of free antigen and imaging tracers **(Figure 5A&B)** that recapitulates our primary experimental findings in mice and predicts how these results may translate to clinical practice in humans (details of the model provided in **Supplemental Materials**).

When all LNs and lymphosomes are functioning normally, interstitial fluid is absorbed by nearby initial lymphatic capillaries that drain locally into collecting lymphatic vessels that pump the lymph to the DLN and eventually return it to the blood circulation. Normally, a local equilibrium exists in which interstitial fluid pressure remains low—near or just below atmospheric pressure—and little lateral movement of fluid occurs in the superficial tissue layers. In contrast, **Figure 5C-F** shows how disabling various combinations of the IN, AX, BR, and PO nodes in the mouse diverts flow to adjacent lymphosomes due to the lack of local pressure minima provided by lymphatic drainage. In general, disabled collecting lymphatic vessels lead to the accumulation of interstitial fluid and then its redirection to the next adjacent lymphosome – even across the midline. This transport can occur through the tissue interstitial space or through the non-valved, highly interconnected lymphatic capillary network. However, the DLN(s) for the adjacent lymphosome might be relatively distal, helping to explain our in vivo data in models of CLND. This computational model predicts that antigen can activate immune responses in specific distal LNs in the body after LN resections.

Our results in a human model (**Figure 5G-I**) were qualitatively similar to those in mice, but important differences arise because of the relative size of the lymphosomes, anatomical connectivity of the vessels, and the degree of redundancy in the lymphatic networks. The pressures in the skin obtained from the full, 3-D human model were compared to an analytical result for a planar, circular lymphosome with the same surface area (**Figure 5J**) in **Figure 5K**. Close agreement is seen despite the planar model not accounting for the spatial curvature of the human chest. Dimensional analysis of the governing equations (see **Supplemental Materials**) revealed that the lateral distance over which interstitial fluid must flow in the skin before being absorbed by functional lymphatics increases with the fluid mobility in the initial, valveless lymphatic vessels (tissue permeability κ or hydraulic conductivity), but decreases with the fluid conductance of the blood vessel and lymph vessel walls.

To examine the size dependence of the lymphosome, we performed a parametric study of the simplified model **(Figure 5L)**. Here, we found that larger lymphosomes, such as those present in humans, generate more total fluid that must be drained and result in higher interstitial pressures than expected in mice. This size difference alone may account for much of the relative difficulty in creating experimental models of lymphedema in laboratory mice. An additional result of the simplified model **(Figure 5M)** was that the mobility of the fluid (κ) in the network of initial lymphatic vessels strongly affects the interstitial fluid pressure, but has little influence on the total quantity of antigen-carrying fluid diverted elsewhere or its destination. Increasing κ by a factor of 10,000 resulted in an increase in the velocity of interstitial flow at the perimeter of the disabled lymphosome by only a factor of about 15 because changes in pressure gradient were offset by changes in κ. For a wide range of parameter values, fluid was diverted to the same nearest neighboring drainage basins.

However, anatomical differences between mouse and human alter the path of flow in the collecting vessels. For example, the direct connection from the inguinal region to the axillary region that exists in the mouse is absent in human. Disabling an AX LN in a human did not affect drainage to the inguinal basin, but like the mouse diverted fluid to contralateral LNs **(Figure 5I)**. Moreover, disabling a single AX LN in a human did not produce the same extensive re-routing of flow seen in the mouse because the human has numerous nodes in the axillary region that form a redundant network. Note that anatomical variations in the network can exist between individuals, and this will affect the flow redundancy.

Administration of ICB to distant LNs enhances efficacy after TDLN dissection

353 Previous preclinical investigations demonstrated that directly delivering a low dose of ICB
354 agents to TDLNs can achieve superior outcome compared to systemic delivery[36,37]. After tumor
355 resection, local intradermal injection of low-dose anti-CTLA4 antibody into the lymphatic
356 drainage basin to the SLNs can activate CD8 effector T cells while decreasing Treg frequency
357 prior to SLNB in patients[39]. These findings highlight the potential of LNs to be used as an ICB
358 target site. Because distant LNs are more likely to be exposed to tumor antigen after LN
359 dissection (**Figure 3 & Supp Figure 2**), we assessed the importance of contralateral LNs for
360 low-dose ICB treatment in mice that have undergone CLND. Since anti-CTLA4 and anti-PD-1
361 combination has shown efficacy in clinical settings[54], we delivered this ICB combination at low
362 dose (5mg/kg) by intradermal administration in a lymphatic basin that is drained by ipsilateral
363 LNs (tumor draining IN+AX) in sham LN surgery mice or contralateral LNs in CLND mice.
364 Compared to isotype IgG, we found ICB drastically increases the volume of ipsilateral LNs in
365 sham LN surgery mice and contralateral LNs in CLND mice (**Figure 6A**). Additionally, these
366 LNs share similar T cell composition (**Figure 6B**) and possess comparable abundance of stem-
367 like effector memory T cells (CD44+, PD-1+, TCF1+, CD39-, CD62L-) which are key
368 contributors to ICB response[55] (**Figure 6C**). Altogether, similar to TDLNs, distant LNs can be
369 activated by ICB in mice after CLND.

370 To directly test the potency of distant LNs during ICB treatment, we treated sham LN surgery
371 and CLND mice bearing E0771 tumors with anti-CTLA4 and anti-PD-1 antibodies (5mg/kg) by
372 intraperitoneal (IP) administration or intradermal administration to contralateral LNs (C.LNs).
373 Strikingly, compared to systemic delivery, combination ICB given to C.LNs provides greater
374 survival benefit and response rate in CLND mice, but not in sham LN surgery counterparts
375 (**Figure 6D**). These results provocatively suggest that delivering ICB therapeutics to downstream
376 or distant LNs may benefit patients that have undergone LN surgery. Notably, CLND decreased
377 ICB efficacy in the systemic anti-CTLA4/PD-1 treatment setting, which may be attributed to the
378 robust response rate (~75%) in this experiment, which is not normally observed clinically[38,56-59].
379 In trial NCT01844505, compared to single agent treatment, the combination of nivolumab and
380 ipilimumab generated a superior response in patients with untreated advanced melanoma[54].
381 However, in trial NCT03068455, compared to nivolumab alone, this combination given in the
382 adjuvant setting did not improve outcome in patients with completely resected melanomas[60].
383 Thus, primary tumor and/or TDLNs may be required for CTLA4 inhibition to provide additional
384 survival benefit when combined with PD-1 inhibition.

385 Compared to adjuvant-only regimens, neoadjuvant-adjuvant ICB can provide better outcomes for
386 patients with advanced melanoma[61]. To examine whether LN surgery compromises neoadjuvant-
387 adjuvant ICB efficacy, B16F10 tumors expressing Gaussia luciferase (B16F10-Gluc) were
388 treated with ICB delivered to the TDLN, and curative primary tumor resection with or without
389 LN surgery (SLNB or CLND) was performed (**Figure 6E**). Mice were monitored for tumor
390 recurrence and metastases (Gluc activity) for 100 days. After 100 days tumor-free mice were
391 rechallenged with B16F10-Gluc cells, and mice that developed tumors were treated with
392 adjuvant ICB delivered to the TDLN (IN LN in no LN surgery condition, AX LN in SLNB
393 condition and contralateral IN LN in CLND condition) (**Figure 6E**). Interestingly, after surgery,
394 ICB, but not IgG, induced vitiligo, especially, at the surgery sites of both primary tumor
395 resection and LN surgery (**Figure 6F**). The appearance of vitiligo indicates that the ICB-induced
396 immune response to antigens involved in melanin production is not abolished by removal of
397 TDLNs and can disseminate beyond the primary tumor location[62]. After neoadjuvant treatment,
398 only one mouse in the No LN surgery + ICB condition had a spontaneous recurrent tumor and
399 one mouse in the SLNB + ICB condition died due to a cause unrelated to cancer (**Figure 6G**),
400 demonstrating the potency of curative surgery. Upon rechallenge, compared to naïve mice, all
401 surgically treated mice exhibited immune memory against the original tumors, while ICB-treated
402 mice possessed greater immune memory compared to IgG-treated counterparts (**Figure 6H**). At
403 this sample size (~15 mice), neither SLNB nor CLND significantly diminished the ICB-induced
404 immune memory or survival benefit (**Figure 6H&I**). Surprisingly, these results suggest that, in a

405 TDLN targeted neoadjuvant-adjuvant ICB treatment regimen, LN surgery along with curative
406 primary tumor resection does not ablate the formation of immune memory against cancer cells
407 and improvement of overall survival.

408 **LN-egressing immune cells are expendable for long-term anti-tumor immune memory**

409 Complete responders emerged after ICB treatment in sham LN surgery and TDLN resected mice
410 (**Figure 2&6**). To evaluate the long-term immune memory, we re-introduced E0771 cells to the
411 original tumor sites of anti-PD1 treatment complete responders (**Figure 2**). Survivors in both
412 sham LN surgery and TDLNs removed conditions rejected tumor rechallenge (**Supp Figure 4A**).
413 To further test whether this immune memory is systemic, E0771 cells were introduced to both
414 ipsi- and contra-lateral sides of animals. Similarly, all survivors, regardless of the presence of
415 TDLNs, remained tumor-free (**Supp Figure 4B**). Finally, we determined that this immune
416 memory is tumor specific, as E0771-immune mice cannot reject B16F10 tumors implanted in
417 either mammary fat pad or dermis (**Supp Figure 4C**).

418 Lymphocytes use sphingosine 1-phosphate (S1P) signaling to exit lymphoid organs including
419 bone marrow, LNs and Peyer's patches[63-65]. We aimed to test whether central memory T cells
420 from LNs enter the circulation and greatly contribute to long-term immune memory in tumor-
421 free survivors. To that end, tumor naïve control mice or complete responders generated by ICB
422 combo treatment (**Figure 6**) were fed with water with or without FTY720 (2.5µg/ml), a potent
423 inhibitor against S1PR[66]. Subsequently, E0771 tumors were implanted to both the primary tumor
424 location and the contralateral site for re-challenge. FTY720 treatment drastically reduced CD4,
425 CD8 and central memory (CD44+/CD62L+) T cells in the circulation ~90% (**Supp Figure 4D)**,
426 suggesting this treatment can block T cells egress from lymphoid organs including LNs.
427 Intriguingly, the vast majority of complete responders remained tumor-free, except two mice
428 from the conditions-one from sham LN surgery and one from CLND-treated with FTY720
429 (**Supp Figure 4E**). Like previous observations (**Supp Figure 4 A&B**), LN surgery status did not
430 affect the immune memory (**Supp Figure 4E)**. Strikingly, this anti-tumor immune memory did
431 not only reside within primary tumor tissues, as subsequent E0771 tumors implanted ectopically
432 in the dermis of these tumor-free survivors from the orthotopic rechallenge study were also
433 rejected (**Supp Figure 4F)**. These findings suggest that ICB-induced anti-tumor immune
434 memory cells spread systemically in complete responders, and the contribution of immune cells
435 egressing from lymphoid organs is dispensable after memory responses have formed.

436 **Distant LNs are reactive after resection of tumor and disease-related LNs in head and neck**
437 **cancer patients treated by ICB**

438 To test whether, after LN dissection, distant LNs contribute to ICB efficacy on suppressing
439 cancer recurrence in patients, we investigated head and neck cancer patients treated by ICB that
440 tend to have a high local recurrence rate[67]. We examined a recent phase I/Ib trial
441 (NCT03635164) in which HPV negative head and neck cancer patients that received neoadjuvant
442 treatment to manage gross disease (primary and grossly involved nodes) consisting of
443 combination hypofractionated radiotherapy and durvalumab (targeting PD-L1). Following a
444 recovery time ranging from 5-6 weeks in the extension cohort, patients underwent surgical
445 resection of the primary tumor and bilateral neck dissection per standard of care. Those with
446 major pathological response or complete pathological response to neoadjuvant radiotherapy and
447 durvalumab were classified as responders (response>95%). Under permission of multi-
448 disciplinary tumor board, with the exception of four cycles of durvalumab, all other adjuvant
449 therapy in the form of radiation or chemotherapy was omitted in responders[68]. To date, no
450 recurrent disease was detected in these responders during post-operative follow-up visits (>2
451 years). We compared CT and PET images at diagnosis to post-surgery follow-up examinations in
452 the responder cohort. Strikingly, after removal of the tumor and initial TDLNs, enlargement of
453 distant LNs was found in most responders, but not in non-responders (**Figure 7A**). Of note, no
454 nodal disease was detected by radiology-guided biopsy, indicating these enlarged LNs were
455 activated and immune-reactive. The reactive LNs were higher echelon LNs in areas that were

now draining the original tumor site. For instance, in patients 01-013 and 01-015, lower neck LNs (posterior cervical) and upper neck LNs (submandibular and submental) were enlarged, respectively, at follow-up, which was not observed at diagnosis (**Figure 7B**). Similarly, in patient 01-009, neck draining mediastinal LNs above the aortic arch were inflamed after tumor and LN resection (**Figure 7C**). These data suggest that surgical removal of the primary tumor and TDLNs can result in reactive distant LNs and extend ICB response in patients.

Discussion:

TDLNs are exposed to high antigen burden, allowing them to readily generate adaptive immune response against cancer cells[19]. Recent reports using mouse tumor models advocate that TDLNs are indispensable for ICB response[1,2,35,69], likely due to unique tumor-specific T cell memory populations[35]. A phase II trial (NCT03698019) of patients with resectable stage III or stage IV melanoma, neoadjuvant-adjuvant pembrolizumab treatment provided improved event-free survival compared to adjuvant-only setting[61], indicating the presence of the primary tumor and/or related LNs is important for optimal ICB response. However, clinical trials involving patients with completely resected stage IIIb/c or stage IV melanoma, demonstrate that patients still benefit from ICB treatment after sentinel LNs and bulky disease-related LNs removal[59,60,70], arguing TDLNs are not necessary for ICB response. Further, retrospective analysis of stage III melanoma patients demonstrates that patients benefited similarly from adjuvant ICB, regardless of the extent of LN surgery. Recent work from our lab and others has shown that metastatic TDLNs are immune suppressed and can impair systemic anti-cancer immune responses[20-22]. Ultimately, the metastatic burden in TDLNs may determine whether SLNB or CLND has a positive, negative or neutral effect on disease recurrence and survival. Because human LN chains are complex with multiple echelons[71], it is key to determine immune activation or suppression status of LNs downstream of sentinel LNs. Identifying LNs with sufficient exposure to antigen but not suppressive factors from tumor, may identify optimal target sites for immunotherapy delivery.

In this study, we emphasize the dynamic and adaptive aspect of antigen transportation. Disruption of normal lymphatic drainage drives the antigen-carrying fluid to flow to adjacent lymphosomes and induces immune response in the LNs of that lymphosome. Often these LNs could be quite distant (and thus non-intuitive) from the original TDLNs, which is corroborated by clinical observations[49,50]. However, the maximal transport distance of interstitial antigens, without being substantially diluted and degraded, remains to be determined. Further, limits of active transport of APCs from the tumor site are also indeterminate. Understanding these spatial limits can explain the anatomic distribution of LNs for regional immune surveillance. Intriguingly, we found CLND induces tumor-specific T cells enrichment in distant LNs, when performed along with primary tumor resection (adjuvant setting). The antigen source fueling the tumor-specific T cell response in distant LNs is unknown. Conceivably, antigens were vastly spread by the surgery, from residual cancer cells at the primary tumor site, or in occult metastatic sites. Despite the importance of antigen trafficking to distant LNs, direct T cell priming in the local tumor microenvironment[72] and tertiary lymphoid structures[73] may also contribute to residual ICB response.

The finding that long-term anti-tumor immune memory is not predominantly reliant on the T cell egress from LNs (**Supp Figure 4**), leads to critical unanswered questions. Do anti-tumor immune memory cells disseminate from TDLNs immediately and accumulate systemically during ICB? Or is systemic immune memory mainly formed after primary tumor clearance? Our neoadjuvant-adjuvant ICB study (**Figure 6**) demonstrated that mice that underwent curative surgery had systemic immune memory development, indicating immune reactions are present at the time of tumor resection. This also suggests that adjuvant ICB may act through existing anti-tumor tissue-resident immune memory cells at the time of treatment. One caveat of the FTY720 experiment to block T cell egress, including memory T cell egress, from LNs is that tissue-resident memory cells can enter the circulation and reject tumor cells at distant sites[74]. S1P

507 inhibition mainly blocks lymphocytes egress from LNs and bone marrow[63] not other tissues, and
508 circulating memory cells are still present in FTY720 treated mice. It is possible a small number
509 of cancer-specific memory clones are sufficient to suppress recurrence. Additionally, S1P
510 metabolism promotes metastasis via activating cell-autonomous signaling pathways such as the
511 C3 complement pathway[75] or PAK1/LIMK1/Cofilin1 pathway[76] in cancer cells, which adds
512 another caveat of using systemic S1P inhibition.

513 Additional limitations are present in our preclinical model when used to address clinical
514 questions[77]. In this work, surgery of skin LNs in mice was used to recapitulate SLNB and CLND
515 procedures. However, large scale and anatomical differences are present between humans and
516 mice. On one hand, the size of a mouse is comparable to a human axilla, thus, the murine version
517 of CLND used in this work may be similar to a SLNB scenario in patients. On the other hand,
518 compared to simple chains of a few LNs in mice, humans have more complex and interconnected
519 lymphatic networks as well as multiple LNs draining one common region[71]; hence, removing a
520 single LN in mice may equate to CLND in human. Encouragingly, consistent with our preclinical
521 data, compensatory lymphatic drainage[49,50], even in the presence of lymphedema[48,78], and distant
522 LN activation are observed in cancer patients (**Figure 7)**. Further, it is important to investigate
523 lymphatic drainage patterns after non-skin LN dissection as ICB treatment increases survival in
524 non-small cell lung cancer[79] and colorectal cancer[80] patients. Notably, regional specification is
525 found in immunity generated in DLNs[81]. Therefore, after CLND, activated T cells in distant LNs
526 may not be able to infiltrate the cancer lesion, which is dictated by anatomic location[81]. In
527 contrast to preclinical studies, clinical trials are more statistically powered[82]. Thus, it is
528 conceivable that LN dissection can cause a statistically significant difference in ICB-mediated
529 survival in trials, whereas the biological impact of this difference is expected to be marginal.
530 Emergence of more powerful biomarkers for patient stratification can enhance ICB response in
531 specific patient cohorts and may exacerbate the effects of LN dissection. Finally, dissection is
532 performed on SLNs and metastatic LNs which are immunosuppressed[83] with disrupted CD8 T
533 cell responses[84]. Consequently, the net benefit of removing these immune suppressive LNs is
534 likely to outweigh the marginal decrease in systemic response to ICB.

535 **Method:**

536 **Cell lines**

537 Parental E0771 (ATCC, CRL-3461), mammary carcinoma line, and parental B16F10 (ATCC,
538 CRL-6475), melanoma line, were obtained from ATCC. All cells were cultured using
539 Dulbecco's modified Eagle's medium (DMEM) (Corning, Cat#10-014-CV) supplemented with
540 10%(v/v) fetal bovine serum (GeminiBio, Cat#100-106) in Forma Steri-cycle incubator (Thermo
541 Scientific, Cat#381), where the CO_2 concentration was set at 5% and temperature was set at
542 37 °C. Cells were trypsinized (Gibco, Cat#25-050-CI) and passaged at a 1:5 ratio when reaching
543 80-90% confluency. All cells were authenticated before use and checked for mycoplasma
544 monthly using PCR Mycoplasma Test Kit I/C (Promokine, Cat # PK-CA91-102).

545 **Transduction**

546 HEK293 cells were transfected with 1μg of plasmids of gene of interest as well as psPAX2 and
547 VSVG, using 5% Fugene transfection reagent (Promega, Cat#E2311) diluted in Opt-MEM
548 (Gibco, Cat#11058-021). After overnight incubation, media containing transfection reagents was
549 replaced with fresh culture media. After another 2 days, lentiviral supernatant was collected,
550 filtered and applied with polybrene (8μg/ml) to target cells.

551 pLV-Ef1a-ZSgreen-SIINFEKL-IRES-puro plasmid (a gift from Stefanie Spranger lab at MIT)
552 was used to generate ovalbumin (257-264) overexpressing cells. CSCW-mbGluc-biotin-IG
553 plasmid (generated by MGH Vector Core)[85] was used to generate Gaussia luciferase expressing
554 cells.

555 **Animal models**

556 In addition to wild-type C57Bl6 mice, lymphotoxin alpha knockout mice B6.129s2-Lta^{tm1Dch}/J
557 (the Jackson Laboratory, Strain# 002258) were used for tumor immunology and dextran
558 trafficking study. Animal experiment protocols were approved by the Institutional Animal Care
559 and Use Committee of the Massachusetts General Hospital, Boston, MA.

560 **Tumor study and ICB administration**

561 200,000 E0771 cells or 500,000 B16F10 cells were trypsinized and resuspended in DMEM base
562 media before implantation. E0771 cells were injected to 4th mammary fat pad of female C57BL6
563 mice while B16F10 cells were injected to the dermis (atop bottom flank) of male or female
564 C57BL6 mice. After 7 days, anti-PD1 blocking antibody (Bio X cell, Cat# BP0146) at 10mg/kg
565 was given intraperitoneally or anti-PD1 and anti-CTLA4 (Bio X cell, Cat# BP0131) blocking
566 antibodies each at 5mg/kg were given intraperitoneally or intradermally. Additional ICB was
567 administered on day 10 and 13 for E0771 tumors or day 9 and 11 for B16F10 tumors. In
568 neoadjuvant-adjuvant treatment regimen, the adjuvant ICB was given when secondary tumors
569 reach the size greater than 100mm^3. Rat (Jackson ImmunoResearch Lb, Cat#012-000-003) and
570 Syrian Hamster (Leinco Technologies, Cat# I-444) IgGs were used as control.

571 Tumor volume (ellipsoid shape is assumed) was monitored at least twice a week and mice were
572 sacrificed when tumor volume reached 1000mm^3 or any tumor dimension was greater than
573 15mm, or when ulceration is greater than 4mm in any dimension. Tumor rechallenge was
574 performed on complete responders, which were defined as mice that remained tumor free for at
575 least 60 days after initial inoculation. In certain studies, LNs were harvested and volume was
576 measured using caliper (ellipsoid shape is assumed).

577 **Surgical procedures**

578 Primary tumor resection: After anesthesia, the fur growing over the tumor site was removed by
579 hair clippers and hair removal cream and the skin sterilized. A small skin incision was made to
580 begin separating the tumor from the underlying fascia and overlying skin through blunt
581 dissection. The tumor was then excised where necessary. The skin was closed with wound clips
582 that were subsequently removed after 2 weeks when the wound is completely closed.

583 LN dissection: Mice skin was shaved and sterilized by wiping ethanol prior to surgery. A 1cm
584 incision was made to skin atop the inguinal or axillary region, which allowed the surgical
585 removal of either inguinal or axillary and brachial LNs, while a 0.5cm incision was made to
586 popliteal skin to remove the popliteal LN. The skin was closed after LN dissection with wound
587 clips. Mice were let recover for at least 10 days before tumor implantation or tracer injection.

588 Splenectomy: A 1 cm incision was introduced to the right of ventral midline (below diaphragm)
589 to open peritoneal cavity. Splenic arteries and veins were ligated at the splenic hilum with a 3–0
590 silk suture and the spleen was removed. The peritoneum was closed after splenectomy with
591 polydioxanone suture, while skin was closed with wound clips. Mice were let recover for at least
592 14 days before tumor implantation.

593 **Dextran tracing**

594 50mg/ml TRITC-dextran with 4400 Dalton molecular weight (Sigma Aldrich, Cat# T1037-
595 50MG), mixed with 25mg/ml FITC-dextran with 2 million Dalton molecular weight (Sigma
596 Aldrich, Cat# FD2000S-100MG) in a total volume of 20µl, were injected to mammary fat pad,
597 dorsal foot or dermis of mice (specified in text). After 6 hours, ipsilateral and contralateral
598 popliteal, inguinal, axillary and brachial LNs as well as spleens were harvested and stained for
599 microscopy.

600 **Immune cells tracing using Kaede mice**

601 500,000 B16F10-OVA cells were implanted to the lower flank dermis of Kaede mice B6.Cg-Tg
602 (CAG-tdKaede) 5Utr (Riken Bioresource Center, RBRC05737). After 2 weeks, primary tumors

603 were resected, and two doses of 10mg/kg anti-PD1 antibodies were administered
604 intraperitoneally (two days and four days after tumor resection). After another 2 weeks,
605 2,500,000 B16F10-OVA cells were implanted to the primary tumor site as rechallenge.
606 Contralateral inguinal LNs were photoconverted (405nm UV light at 12V/0.09A for 5mins),
607 when recurrent tumors exceeded 100mm^3. After 1 day, recurrent tumors were harvested for flow
608 analysis.

609 **Antigen-presenting cells-based vaccination**

610 Bone marrow was flushed out from hind limbs of 7-12 week old C57Bl6 mice. After ACK buffer
611 lysis, cells were cultured in RPMI media supplemented with 10% FBS, 1% Pen/Strep, 50μM β-
612 mercaptoethanol, 20ng/ml GM-CSF (PeproTech, Cat# 315-03) and 10ng/ml IL-4 (PeproTech,
613 Cat# 214-14). Media was refreshed every three days to generate BMDCs. At day 9, BMDCs
614 were pulsed with 20μg/ml $OVA_{257-264}$ (Invitrogen, Cat# vac-sin) for 3 hours, then 2μg/ml LPS
615 (Sigma, Cat# L-2630-10MG) was added as adjuvant. The next day, 500,000 activated BMDCs
616 (in 20μl DMEM base media) were collected and injected to the foot of C57Bl6 mice that
617 underwent sham surgery or LN surgery. After 7 days, LNs were harvested from immunized mice
618 for further analysis.

619 **Immunofluorescence staining and imaging**

620 Fresh tissue was embedded in OCT compound (Tissue-Tek, Cat# FIS 23730571) and frozen at -
621 80 °C for overnight. Subsequently, frozen tissue was cut into serial sections with 10μm interval
622 using cryostat station. 3-5 tissue sections representing different tissue depths were used for
623 staining. Tissue sections were fixed using 4% paraformaldehyde for 15mins at room temperature.
624 After fixation, slides were rinsed in PBS-T and blocked in 5% normal donkey serum for 1 hour.
625 Then slides were stained with primary antibody in humidity chamber for overnight at 4 degree.
626 Next day, primary antibody was washed away, and slides were incubated with secondary
627 antibody for 1 hour at room temperature. At last, DAPI was added to label DNA and slides were
628 mounted. Slides were imaged using Olympus IX81 fluorescence microscope with FV10-ASW
629 4.2 software or ZEISS Axio scan Z.1 with ZEN 2.3 slidescan software.

630 **Flow cytometry**

631 Fresh tissue was dissociated and filtered using 70μm mesh. Red blood cells were lysed by
632 incubation with ACK lysis buffer for 2 minutes, followed by neutralization using PBS with 10%
633 FBS. Next, samples were stained with viability dye: DAPI or Zombie Violet (1:200) (Biolegend,
634 Cat# 423113) for 15 mins, then blocked by Fc receptor (CD16/32) antibody (1:500) (Biolegend,
635 Cat# 101302) for 15 mins. After blocking, samples were stained with primary antibody (or
636 tetramer) for 1 hour at 4 °C in the dark, then washed with PBS and fixed using BD fixative. At
637 last, samples were analyzed by Fortessa X20 cytometer within two weeks of fixation.

638 **Image processing**

639 All image processing of fluorescence images was done in ImageJ (https://imagej.nih.gov/ij/) or
640 QuPath (https://qupath.github.io) to adjust brightness and contrast. Constant adjustment setting
641 was done to all images from individual experiment. For signal quantification, Cellprofiler
642 (https://cellprofiler.org) and Qupath were used. To be specific, the tissue border was identified
643 from each image manually. Specific staining fluorescence signal was identified by adaptive
644 thresholding-minimum cross-entropy-algorithm. Positive signal objects were de-clumped by
645 intensity (Cellprofiler), or positive cell detection command with manual threshold (QuPath).
646 Another object size-based filter was additionally applied to cell identification (1-10μm) to
647 remove non-specific staining.

648 **Retrospective analysis of melanoma patient survival**

649 We performed a retrospective analysis of patients with stage III cutaneous melanoma according to
650 the 8th American Joint Committee on Cancer criteria. The patients were selected from a large

melanoma cohort study and tumor biobank maintained at Massachusetts General Hospital for over 13 years (2009-2022) and approved by the Institutional Review Board. Informed consent was obtained from all patients. All patients included in this analysis received at least one line of PD1 immune checkpoint blockade adjuvant therapy. For each patient, we extracted general demographic information, histopathological reports, extent of surgery, adjuvant treatments, recurrence and survival outcomes. The data extraction was followed by statistical analysis using R (Core Team 2021) package[86] (survminer) to generate Kaplan-Meier survival curves. Significance was determined using a log-rank test and the p-value is reported on each plot. P-value significance was considered to be $p<0.05$.

Clinical trial data and patient records

In phase I/Ib trial NCT03635164, patient response rate (Laurel Darragh & Sana Karam): Pathological response was evaluated independently by two board-certified pathologists who were blinded to treatment outcome. Specimens collected at time of surgery were evaluated for microscopic residual tumor (only scattered residual foci) or macroscopic residual tumor and scored based on these findings.

In phase I/Ib trial NCT03635164, radiology images (Laurel Darragh & Sana Karam): At baseline, patients received a PET/CT of skull base to mid-thigh and an MRI with and without contrast of the neck no more than 28 days before radiation therapy. Long-term follow up imaging assessment was done with either PET/CT and/or MRI at the discretion of the treating physician. Enlarged lymph nodes at the follow-up timepoints were noted on imaging by a radiologist and concerning nodes were biopsied to rule out recurrence.

Statistics

Statistical significance was determined with either two-tailed unpaired Student's t test (for two conditions) or one-way ANOVA (for conditions more than 2) with Tukey post-hoc adjustment. Log-rank (Mantel-Cox) test was used for overall survival. Data are presented as mean ± SEM. Fisher's exact test was used to analyze contingency tables including responders vs. non-responders and survivors vs. non-survivors. Statistical significance threshold was set at $p<0.05$. All calculation was performed using GraphPad Prism 9 software.

Mathematical modeling

The mathematical model predicts interstitial fluid pressures, flow rates, and the patterns of fluid redistribution after selective disabling of LNs. Details of the model formulation, validations and parameter dependence are available in the **Supplemental Materials**. In summary, our mathematical model focuses on transport of antigen, antigen-presenting cells and tracer by fluid flow rather than molecular diffusion. Relatively small molecules such as the 4k MW dextran take only minutes to diffuse along concentration gradients over the distances between blood vessels or within lymph nodes (~100 μm) so that they can quickly reach the bloodstream for distribution throughout the body. In contrast, larger materials such as 2M MW dextran might take days or longer to diffuse similar distances which means that the larger tracer, free antigens and cells move predominantly by interstitial flow.

Interstitial fluid in the skin is assumed to arise from the semipermeable walls of the capillaries, and then flow locally through the interstitial space to the nearest initial lymphatic capillaries. The initial lymphatic vessels in the skin, which lack intraluminal valves and contractile muscle, form a highly redundant meshwork that carry fluid passively down gradients in the interstitial pressure to the nearest collecting lymphatic vessels which then actively pump lymph toward the sentinel lymph node for that lymphosome of the skin[18]. The boundaries of the drainage basins or lymphosomes are determined by the locations of the collecting vessels and which lymph nodes are downstream.

Antibodies and tetramer

Information (source and concentration) of antibodies and tetramer used in immunofluorescence and flow cytometry are listed in **Supplemental Materials**.

Acknowledgement

This work was financially supported by grants from NIH (K00CA234940 to H.Z.; R21AI097745, R01CA214913, R01HL128168, and R01CA284372 to T.P.P; R01CA284603 to T.P.P., L.L.M. and J.W.B.; 1R01DE028529-01, 1R01DE028282-01, 1R01DE028529-01 and 1P50CA261605-01 to S.D.K.; R35CA242379 to M.G.V.H.), the Rullo Family MGH Research Scholar Award (T.P.P.; G.M.B.), the Patricia K. Donahoe Award from the Huiying Foundation (G.M.B.), and the Adelson Medical Research Foundation (G.M.B.), the Ludwig Center at MIT (M.G.V.H.) and the MIT Center for Precision Cancer Medicine (M.G.V.H.), the Breast Cancer Alliance (J.M.U.), and the Melanoma Research Foundation (J.M.U.). The Phase I/Ib clinical trial NCT03635164 was funded by AstraZeneca, S.D.K also received clinical trial funding from Genentech and preclinical funding from Roche.

Competing Interests

M.G.V.H. acknowledges that he is a scientific advisor for Agios Pharmaceuticals, iTeos Therapeutics, Sage Therapeutics, Pretzel Therapeutics, Lime Therapeutics, Auron Therapeutics, and Droia Ventures. G.M.B has sponsored research agreements through her institution with: Olink Proteomics, Teiko Bio, InterVenn Biosciences, Palleon Pharmaceuticals. She served on advisory boards for: Iovance, Merck, Nektar Therapeutics, Novartis, and Ankyra Therapeutics. She consults for: Merck, InterVenn Biosciences, Iovance, and Ankyra Therapeutics. She holds equity in Ankyra Therapeutics.

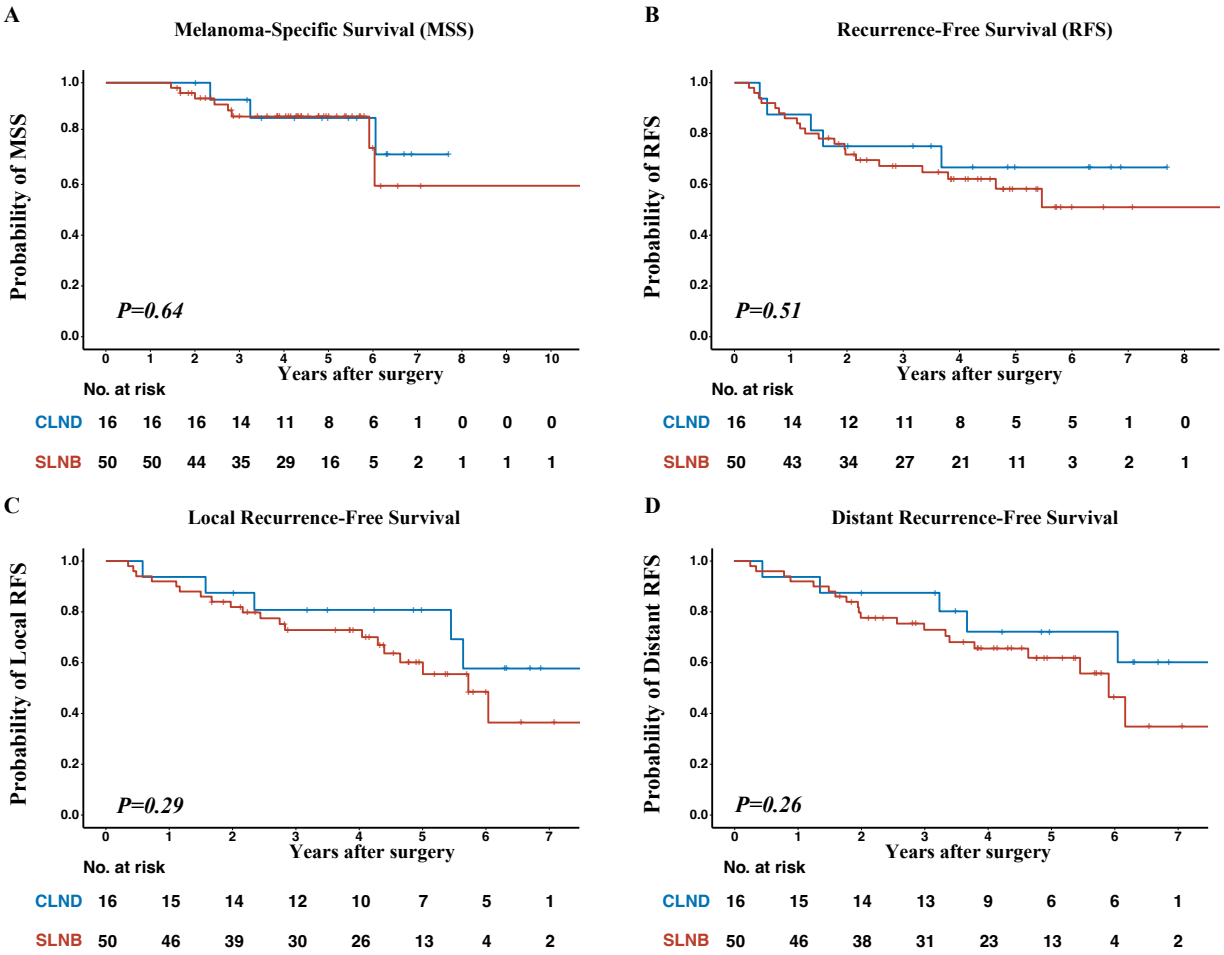

Figure 1. Adjuvant ICB response is not affected by the extent of LN surgery in stage III melanoma patients. Retrospective analysis was performed on a cohort of cutaneous stage III melanoma patients who underwent SLNB or CLND, and were treated by adjuvant nivolumab or pembrolizumab at Massachusetts General Hospital. (**A**) Melanoma-specific survival, (**B**) recurrence-free survival, (**C**) local recurrence-free survival and (**D**) distant recurrence-free survival are plotted.

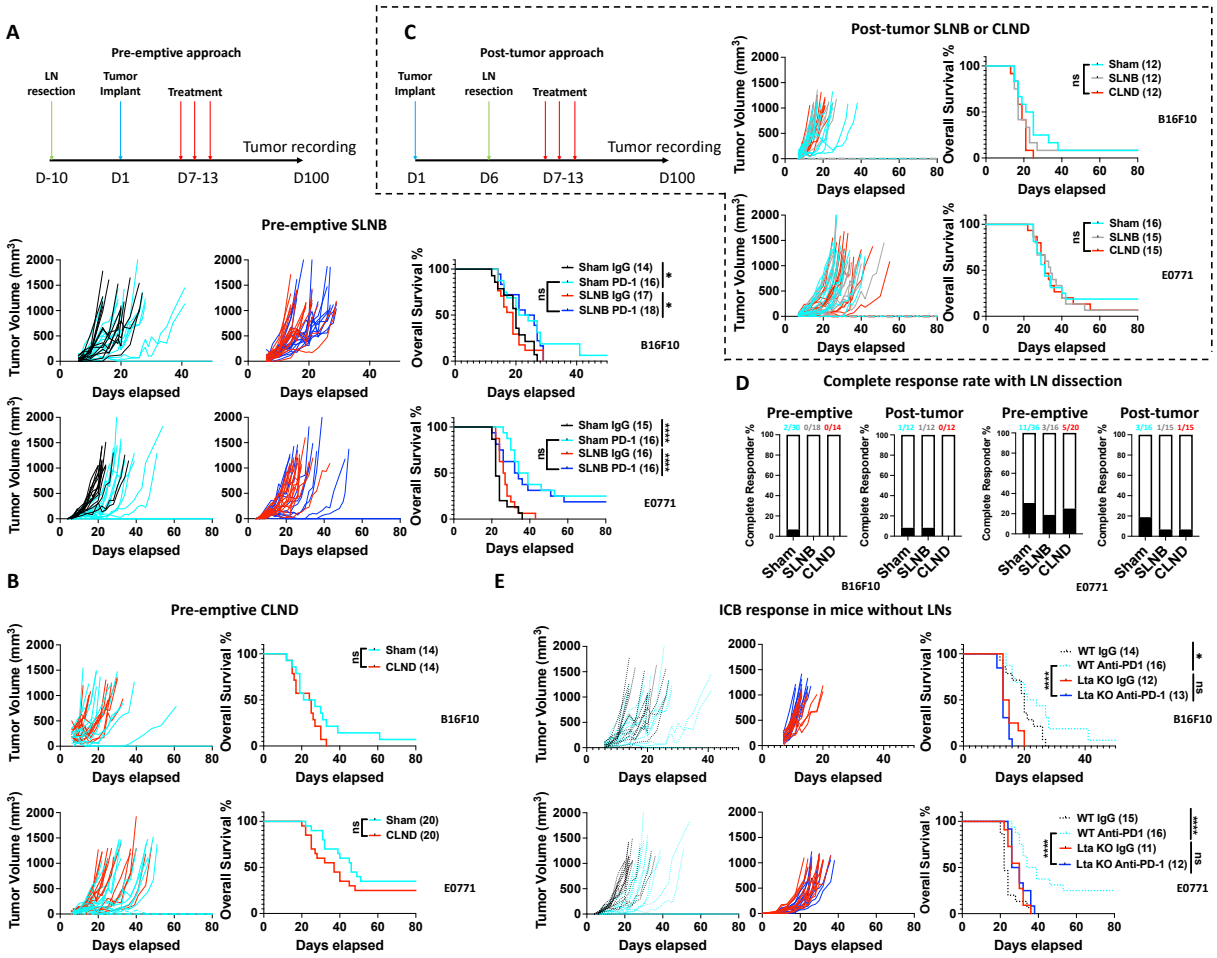

Figure 2. ICB response persists after LN dissection. (**A**) Sham surgery or SLNB was performed on C57Bl6 mice (day -10) prior to orthotopic tumor implantation (day 1). Mice were treated by rat IgG control or anti-PD1 antibody (day 7) three times (every 2 days for B16F10 or every 3 days for E0771, 10mg/kg). Tumor volume (*left & middle*) and overall survival (*right*) were plotted for mice bearing orthotopic B16F10 (*top*) or E0771 (*bottom*) tumors, respectively. (**B**) To evaluate the impact of more aggressive surgery, sham surgery or CLND was performed followed by tumor implantation and subsequent anti-PD1 inhibition using the same regimen described above. Tumor volume (*left*) and overall survival (*right*) were plotted for mice bearing B16F10 (*top*) or E0771 (*bottom*) tumors, respectively. (**C**) In contrast with pre-emptive approach, impact of post-tumor implantation LN dissection was also assessed. After tumor implantation (day 1), sham surgery, SLNB or CLND was performed on C57Bl6 mice (day 6) right before anti-PD1 treatment (day 7). Tumor volume (*left*) and overall survival (*right*) were plotted for mice bearing B16F10 (*top*) and E0771 (*bottom*) tumors. (**D**) Frequency of complete responders from pre-emptive and post-tumor TDLN removal studies were plotted. Fisher's exact test was used for statistical analysis. (**E**) B16F10 (*top*) or E0771 (*bottom*) tumor response to anti-PD1 treatment was tested in Lta^{tm1Dc} mice. ICB response of wildtype (WT) sham mice from (**A**) SLNB study was plotted in dashed lines for comparison. Tumor volume (*left*) and overall survival (*right*) were plotted. In all animal studies, "(n)" indicates number of mice used. Log-rank test with Bonferroni test was used for statistical analysis of survival data. *p<0.05, ****p<0.0001.

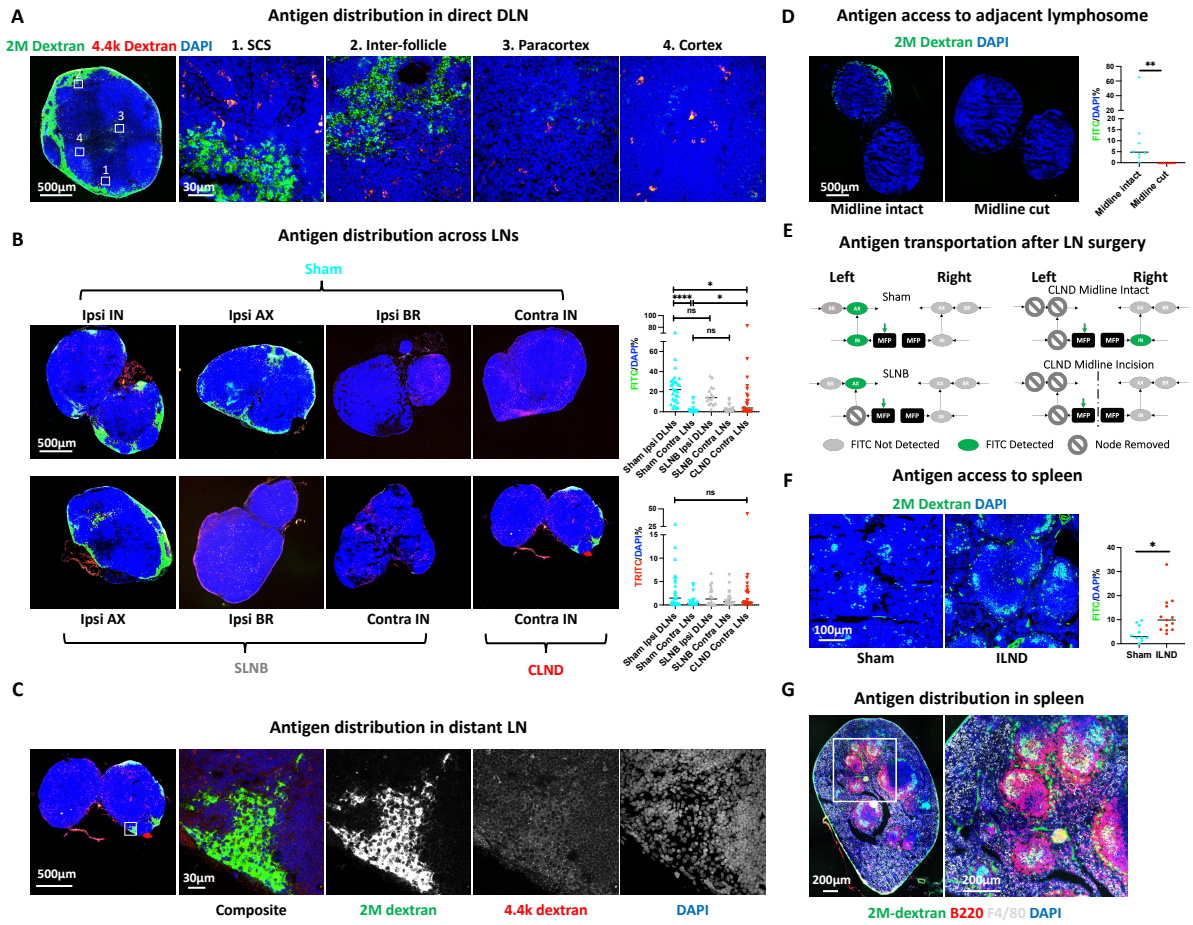

Figure 3. DLN dissection alters lymph drainage and promotes antigen access to distant lymphoid organs. FITC-conjugated 2 million Dalton (FITC-2MD) and TRITC-conjugated 4.4 kilodalton (TRITC-4.4kD) dextran were injected to the mammary fat pad of mice that underwent sham surgery, SLNB or CLND. (**A**) Representative immunofluorescence images of mouse with sham surgery demonstrate intranodal dextran distribution. (**B**) Dextran distribution in ipsilateral inguinal (IN), axillary (AX), brachial (BR) LNs as well as contralateral IN LNs in animals that underwent sham, SLNB or CLND. (**C**) Greater magnification image shows that large dextran molecules enter subcapsular sinus of contralateral IN LN in CLND mice, suggesting transport through lymphatic vessels. (**D**) FITC-2MD dextran distribution in contralateral inguinal LN from CLND mice with or without acute midline skin incision, prior to dextran injection to mammary fat pad. (**E**) Diagram shows lymph flow pattern in various surgery settings. (**F**) FITC-2MD dextran distribution in spleens from mice that underwent sham surgery or ipsilateral LN dissection (ILND). (**G**) Representative immunofluorescence images demonstrate FITC-2MD dextran location in spleen from ILND mice relative to B cells (B220) and macrophages (F4/80). In this figure, fluorescence signal quantification was calculated by the occupied area, while DAPI was used to normalize LN area. Two tailed student t test (two conditions) and one way ANOVA with Tukey post analysis (more than two conditions) were used for statistical analysis. *p<0.05, **p<0.01, ****p<0.0001.

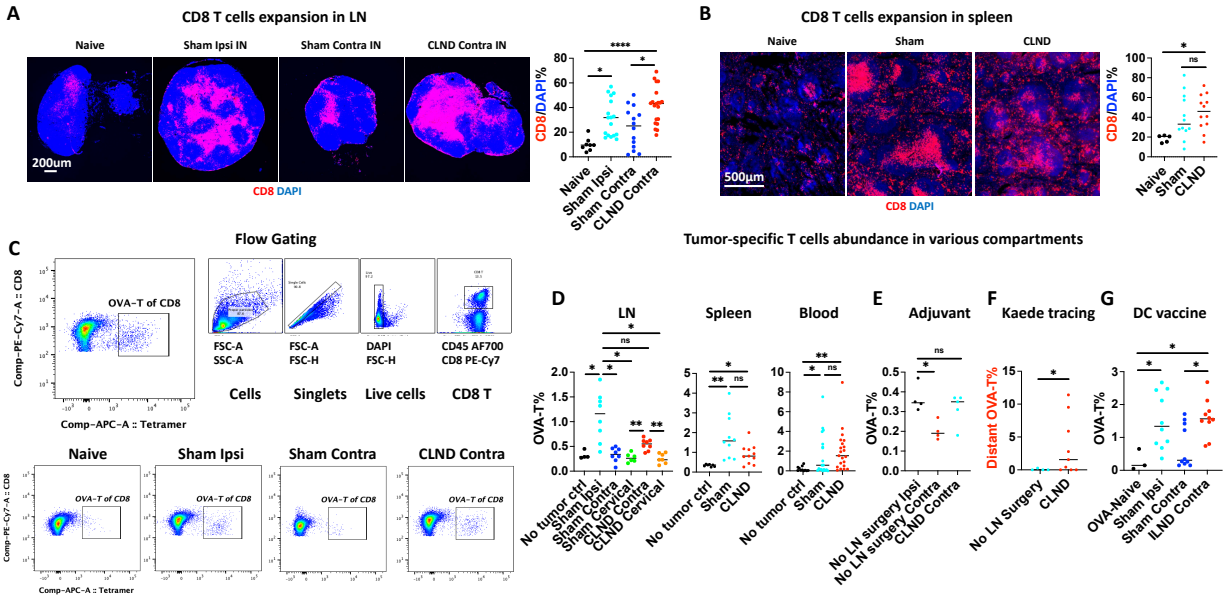

Figure 4. TDLN dissection stimulates immune responses in distant LNs. To assess the tumor-specific T cell response, B16F10 tumors overexpressing Ovabulmin$_{257-264}$ (OVA) were implanted to sham and CLND mice followed by anti-PD1 inhibition. (**A**) In ipsilateral and contralateral LNs as well as (**B**) spleens, CD8 T cell expansion is shown by immunofluorescence images. (**C**) Additionally, OVA-specific CD8 T cells in ipsilateral, contralateral and cervical LNs, spleens and blood were determined by tetramer staining using flow cytometry analysis. Gating approach and representative density plots from ipsilateral and contralateral LNs are shown. (**D**) Abundance of OVA-specific CD8 T cells (CD8+, Tetramer+) is plotted for various LNs, blood and spleens collected from sham and CLND mice; each dot represents data from a single mouse. (**E**) OVA-specific CD8 T cell response in ipsilateral and contralateral LNs is shown in an adjuvant setting where primary tumor resection was performed with or without CLND before anti-PD1 inhibition. (**F**) Similar to **E**, Kaede mice bearing B16F10-OVA tumors were treated by adjuvant anti-PD1 inhibition, followed by tumor rechallenge to primary site. Once recurrent tumor formed, contralateral inguinal LNs were photoconverted prior to tissue harvesting for flow analysis. Abundance of Kaede red+ tumor infiltrating OVA-specific CD8 T cells is plotted. (**G**) To assess antigen-presenting cell-mediated T cell response after LN dissection, BMDCs were pulsed with OVA and LPS for 1 day, and injected to the footpad of mice that underwent sham surgery or ILND. OVA-specific CD8 T cells in ipsilateral and contralateral LNs are plotted. In this figure, fluorescence signal quantification is calculated by the occupied area, while DAPI is used to normalize. Two tailed student t test (two conditions) and one way ANOVA with Tukey post analysis (more than two conditions) were used for statistical analysis. *p<0.05, **p<0.01, ****p<0.0001.

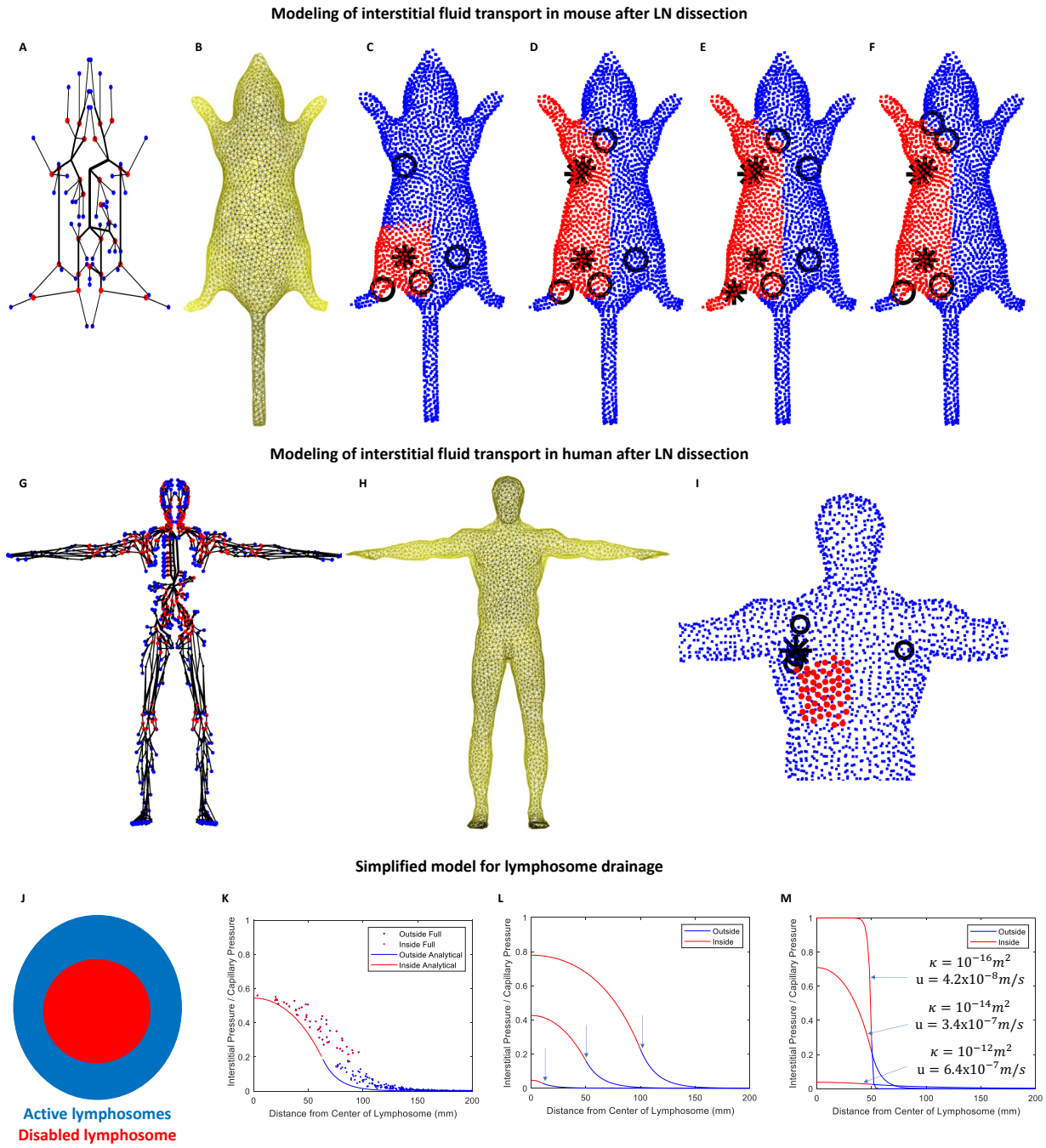

Figure 5. Mathematical modeling of antigen access to adjacent lymphosomes via dermal network after node dissection. (**A**) Mouse model with network of collecting lymphatic vessels (black), collecting points (blue) and lymph nodes (red). (**B**) Computational mesh for network of initial lymphatic vessels in the skin. (**C-F**) Drainage basins (red) with disabled nodes (black *), four most active compensatory nodes (black o) for (**C**) inguinal node resection, (**D**) inguinal and axillary node resection, (**E**) popliteal, inguinal, axillary and brachial node resection, and (**F**) inguinal and axillary node resection with severed midline model (intact **C-E**). (**G**) Human male model with network of collecting lymphatic vessels (black), collecting points (blue) and lymph nodes (red). (**H**) Computational mesh for network of initial lymphatic vessels in the skin. (**I**) Drainage basin (red) with disabled axillary node (black *), four most active compensatory nodes (black o). (**J**) Planar geometry for analytical model with a circular disabled lymphosome (red) surrounded by tissue with active lymph clearance (blue). (**K**) Interstitial pressure inside and outside of the disabled lymphosome from the full, 3D human model compared to an analytical result for the planar

geometry in (**J**) with the same surface area. (**L**) Dependence of interstitial pressure on radius of disabled lymphosome (arrows) showing how small lymphosomes produce little increase in interstitial pressure. (**M**) Dependence of interstitial pressure and fluid velocity u at the periphery of the disabled lymphosome on tissue permeability (radius 50 mm) showing how changes in tissue permeability can alter the interstitial pressure, but barely affects the rate of fluid/antigen flow to compensatory lymphosomes (u).

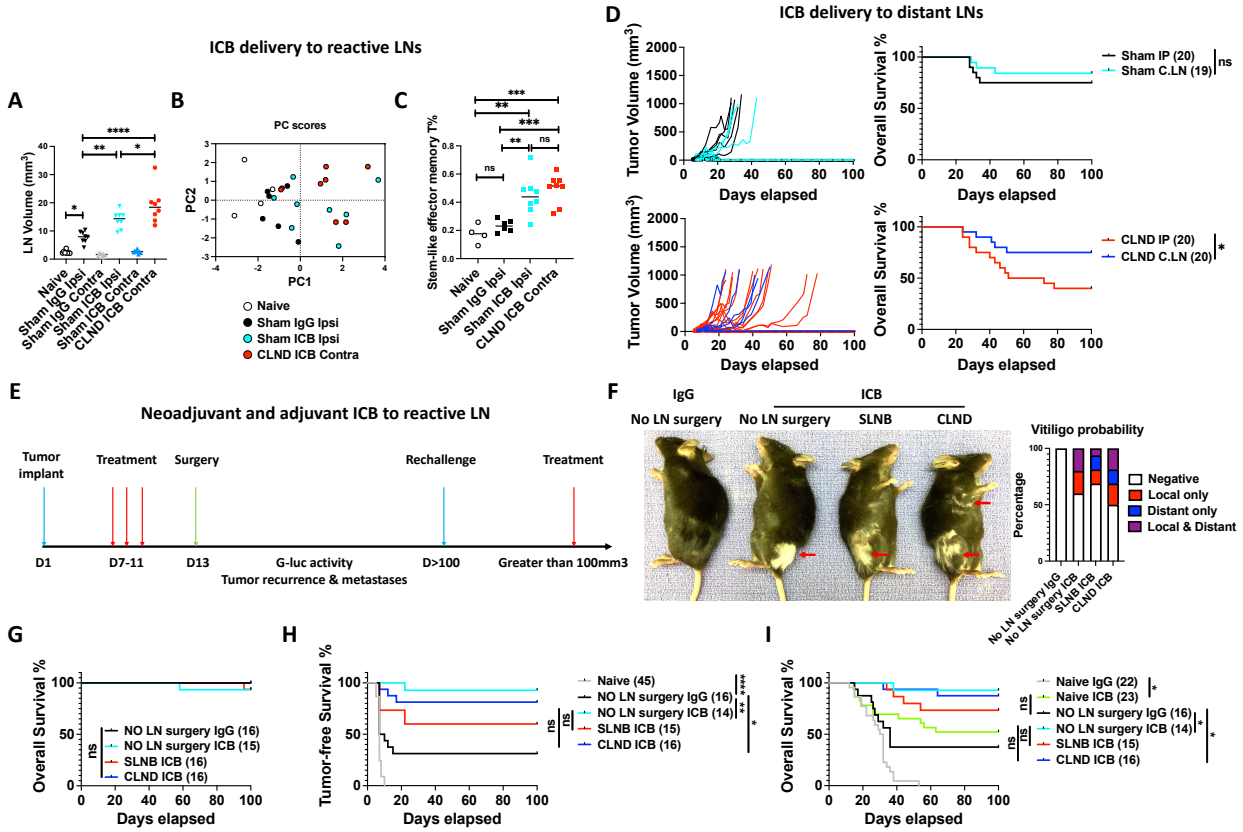

Figure 6. Distant LNs can be targeted to improve ICB response. Sham surgery or CLNB was performed on C57Bl6 mice (day -10) prior to orthotopic E0771 tumor implantation (day 1). IgG control or combination of anti-PD1 and anti-CTLA4 antibodies were intradermally delivered to ipsilateral TDLNs or contralateral LNs in sham and CLND conditions, respectively (day 7) for three doses at 5mg/kg. LNs exposed to treatment were harvested for flow cytometry analysis measuring CD45, TCR-beta, CD4, CD8, CD44, PD-1, TCF-1, CD39 and CD62L. Non-tumor bearing naïve mice are used as control. (**A**) LN Volume of naïve mice or mice treated by IgG or ICB combination is plotted. (**B**) Principle component analysis is performed on naïve or treatment-exposed LNs, using the abundance of antigen-experienced T cells (CD44+, PD-1+), memory T cells (CD44+, PD-1+, TCF1+), central memory T cells (CD44+, PD-1+, TCF1+, CD62L+), effector memory T cells (CD44+, PD-1+, TCF1+, CD62L-), stem-like effector memory T cells (CD44+, PD-1+, TCF1+, CD62L-, CD39-) and their CD4/CD8 subsets. (**C**) The percentage of stem-like effector memory T cells to total T cells is plotted. (**D**) Using the same surgery, tumor implantation and treatment procedure, ICB was given intraperitoneally or intradermally to the lymphatic basin of contralateral inguinal LN (day 7) for three times at 5mg/kg in sham and CLND mice. Tumor volume (*left*) and overall survival (*right*) were plotted. (**E**) Timeline for neoadjuvant-adjuvant treatment and tumor rechallenge. (**F**) Representative images of vitiligo (arrows) that developed in mice after neoadjuvant treatment (*left*). Percentage of mice with local, distant or local & distant vitiligo across conditions (*right*). (**G**) Overall survival of mice treated by neoadjuvant ICB with various LN surgery status. (**H**) Tumor-free survival of mice previously treated by neoadjuvant ICB after tumor rechallenge. Naïve mice were used as control. (**I**) Overall survival of mice previously treated by neoadjuvant-adjuvant ICB after tumor rechallenge. Of note, only mice that developed tumors after rechallenge were given adjuvant treatment. In all studies, "(n)" indicates the number of mice used. One way ANOVA with Tukey post analysis (comparing more than two conditions) and Log-rank test with Bonferroni test (survival) were used for statistical analysis. *p<0.05, **p<0.01, ***p<0.001, ****p<0.0001.

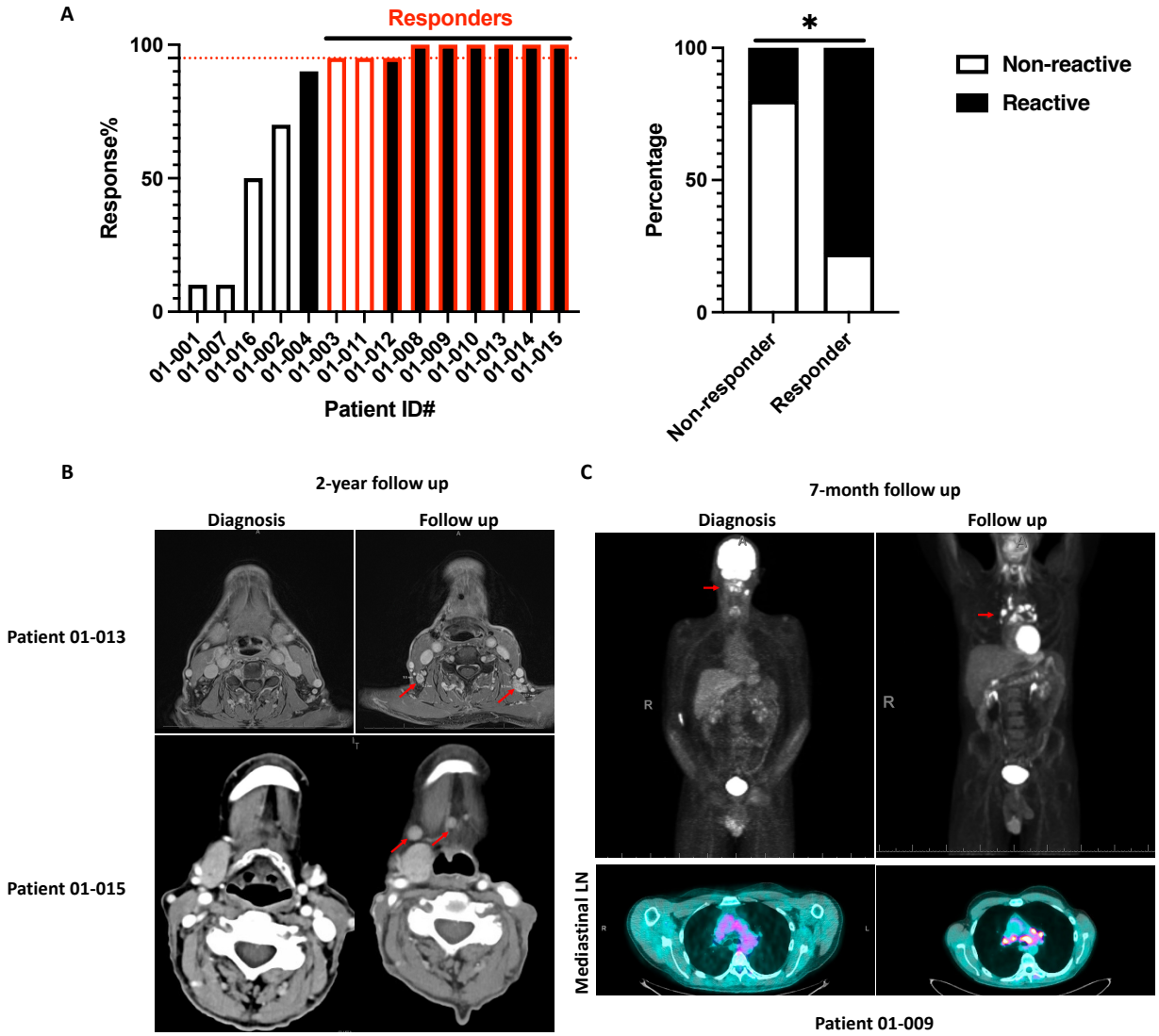

Figure 7. Distant LNs are inflamed after resection of tumor and related LNs in cancer patients. (**A**) *Left*, from phase I trial NCT03635164, response rate and reactive status of remaining LNs after neck dissection are shown. *Right*, percentage of patients that have enlarged or reactive LNs in more distal LN basins are plotted in non-responder and responder cohorts. Fisher's exact test 2x2 is used to evaluate statistical significance, *$p<0.05$. (**B**) CT images of patient 01-013's and 01-015's neck at diagnosis and 2-year post-surgery follow-up scan are demonstrated. Arrows indicate enlarged neck LNs (posterior cervical LNs in patient 01-013; submandibular and submental LNs in patient 01-015). (**C**) CT and PET images of patient 01-009 at diagnosis and 7-month post-surgery follow-up scan. Arrows indicate reactive cervical (diagnosis) and apex mediastinal LNs (follow up).

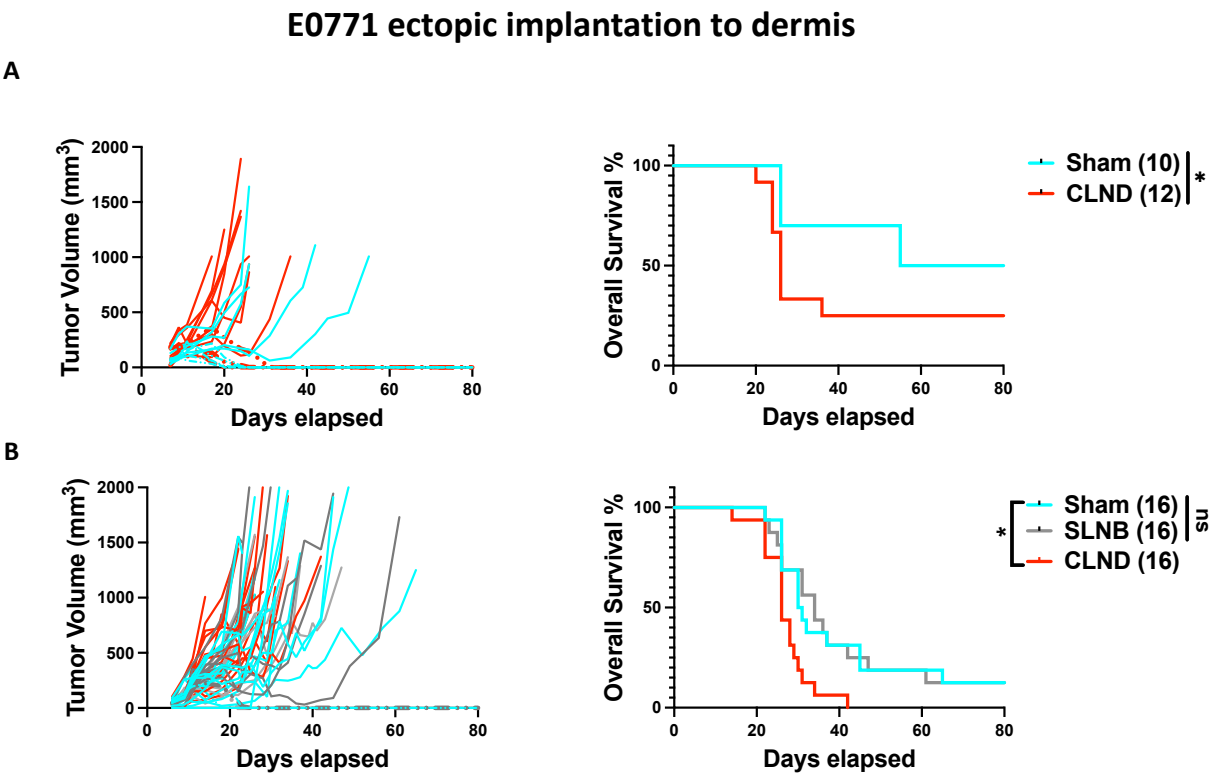

Supplementary Figure 1. Aggressive LN dissection damages ICB response in ectopic setting. (**A**) For pre-emptive setting, sham surgery or CLND was performed on C57Bl6 mice (day -10) prior to E0771 tumor implantation to dermis (day 1). Mice were treated by anti-PD1 inhibition (day 7) for three times at 10mg/kg. Tumor volume (*left*) and overall survival (*right*) were plotted. (**B**) For post-tumor setting, after E0771 tumor implantation to dermis (day 1), sham surgery, SLNB or CLND was performed on C57Bl6 mice (day 6) right before anti-PD1 treatment. Tumor volume (*left*) and overall survival (*right*) were plotted. In all animal studies, "(n)" indicates the number of mice used. Log-rank test with Bonferroni test was used for statistical analysis of survival data. *p<0.05.

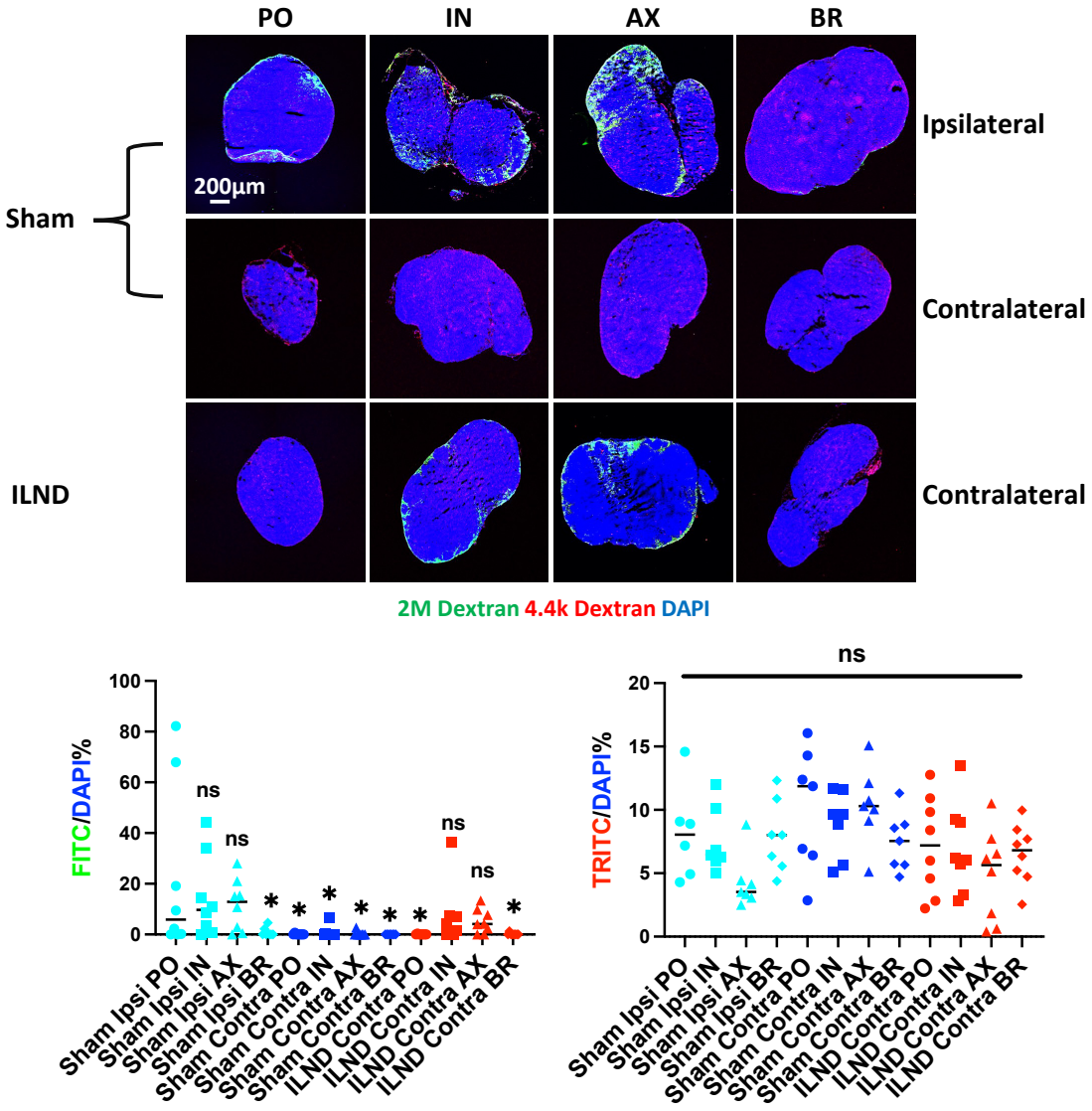

Supplementary Figure 2. Lack of primary drainage promotes antigen to access distant LNs. FITC-conjugated 2 million Dalton (FITC-2MD dextran) and TRITC-conjugated 4.4 kilo Dalton dextran (TRITC-4.4kD dextran) were injected to the footpad of mice have undergone sham surgery or ipsilateral LN dissection (ILND). Representative immunofluorescence images demonstrate dextran distribution in ipsilateral popliteal, inguinal, axillary, brachial LNs as well as contralateral counterparts. In this figure, fluorescence signal quantification is calculated by the occupied area, while DAPI is used to normalize the LN area. One way ANOVA with Tukey post analysis was used for statistical analysis, all conditions were compared to Sham ipsilateral popliteal LN, *p<0.05.

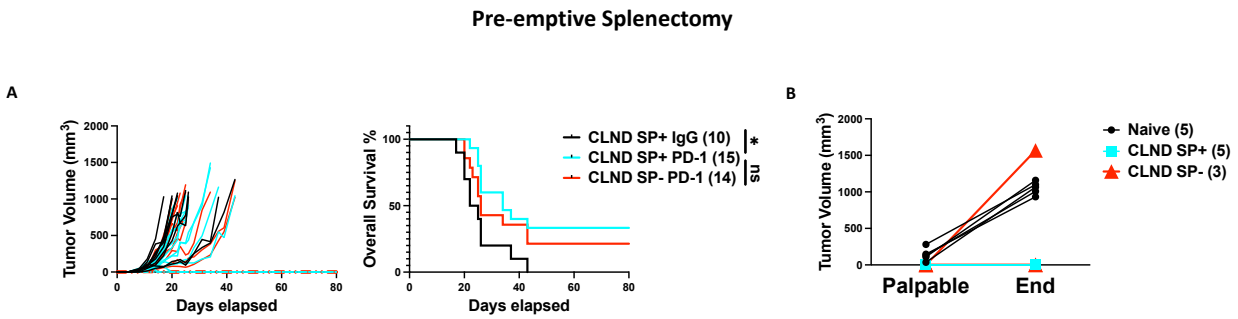

Supplementary Figure 3. Spleen contributes marginally to residual ICB response after CLND. (**A**) Sham surgery (SP+ condition) or splenectomy (SP- condition) was performed on mice 14 days prior to CLND. E0771 tumor implantation and IgG or anti-PD1 treatment were conducted using same procedure as before. Tumor volume (*left*) and overall survival (*right*) were plotted. (**B**) E0771 tumor rechallenge was performed using complete ICB responders. Tumor volume was plotted when tumor was palpable (after day 7) and when the study was ended. In all animal studies, "(n)" indicates the number of mice used. Log-rank test with Bonferroni test was used for statistical analysis of survival data. *p<0.05.

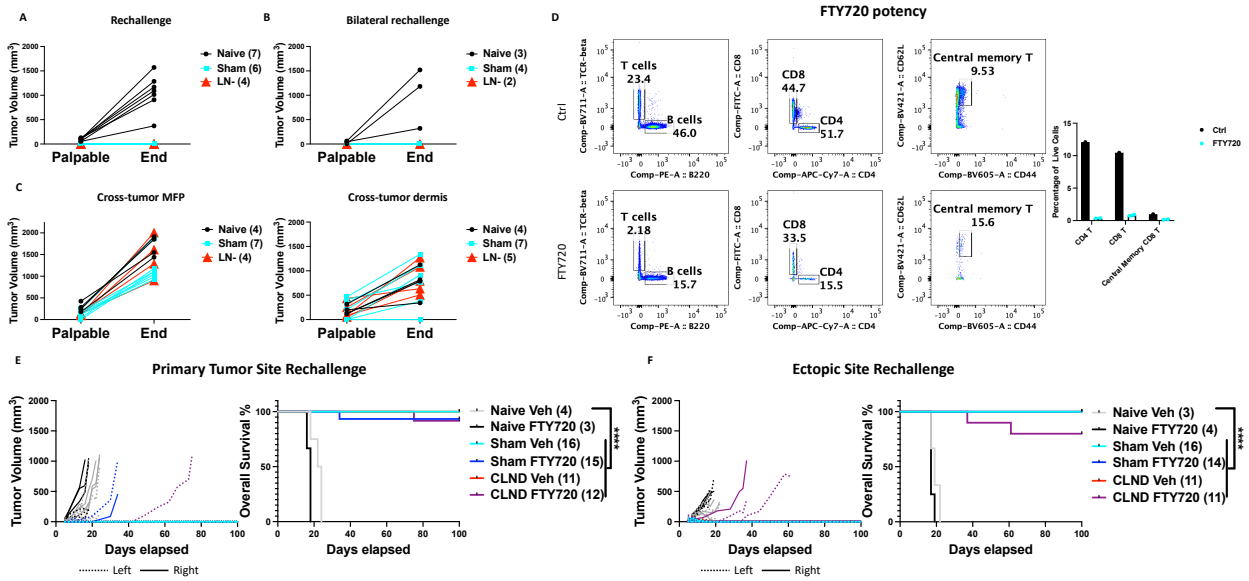

Supplementary Figure 4. LN-egressing immune cells are not necessary for long-term anti-tumor immune memory. (**A-C**) In these rechallenge studies, tumor volume was plotted when tumor was palpable (after day 7) and when the mouse was euthanized. (**A**) E0771 tumors were implanted orthotopically to the primary tumor site of naïve mice or complete ICB responders. (**B**) E0771 tumors were orthotopically implanted to both ipsilateral (primary tumor site) and contralateral sides of naïve mice or complete ICB responders. (**C**) B16F10 tumors were implanted to the mammary fat pad (*left*) or dermis (*right*) of naïve mice or E0771-immune mice. (**D**) To test the potency of FTY720 in depleting circulating lymphocytes, mice were given water containing or FTY720 (2.5ug/ml) for 5 days or maintained on regular water (control). Blood was then collected for characterization. *Left*, representative density plot demonstrates the abundance of circulating B cells (CD45+, B220+), T cells (CD45+, TCR-beta+) and central memory T cells (CD45+, TCR-beta+, CD8+, CD44+, CD62L+). *Right,* quantification of CD4, CD8 and central memory T cells, relative to live cell gate, was graphed. To test the contribution of lymphocytes egressing from lymphoid organs to anti-tumor immune memory, E0771 tumor rechallenge to 4th mammary fat pad (**E**) and dermis (**F**) were performed sequentially on both sides in complete ICB responders fed with vehicle or FTY720 water. Tumor naïve mice were used as controls. Tumor volume (*left*) and overall survival (*right*) were plotted. Of note, dermal tumors were often ulcerated leading to euthanasia. In all animal studies, "(n)" indicates the number of mice used. Log-rank test with Bonferroni test was used for statistical analysis of survival data. ****$p<0.0001$.

883 **References:**

884 1 Fransen, M. F. *et al.* Tumor-draining lymph nodes are pivotal in PD-1/PD-L1 checkpoint
885 therapy. *JCI Insight* **3** (2018). https://doi.org:10.1172/jci.insight.124507
886 2 Zhao, X., Kassaye, B., Wangmo, D., Lou, E. & Subramanian, S. Chemotherapy but Not the
887 Tumor Draining Lymph Nodes Determine the Immunotherapy Response in Secondary
888 Tumors. *iScience* **23**, 101056 (2020). https://doi.org:10.1016/j.isci.2020.101056
889 3 Ishida, Y., Agata, Y., Shibahara, K. & Honjo, T. Induced expression of PD-1, a novel
890 member of the immunoglobulin gene superfamily, upon programmed cell death. *EMBO*
891 *J* **11**, 3887-3895 (1992). https://doi.org:10.1002/j.1460-2075.1992.tb05481.x
892 4 Iwai, Y. *et al.* Involvement of PD-L1 on tumor cells in the escape from host immune
893 system and tumor immunotherapy by PD-L1 blockade. *Proc Natl Acad Sci U S A* **99**,
894 12293-12297 (2002). https://doi.org:10.1073/pnas.192461099
895 5 Brunet, J. F. *et al.* A new member of the immunoglobulin superfamily--CTLA-4. *Nature*
896 **328**, 267-270 (1987). https://doi.org:10.1038/328267a0
897 6 Leach, D. R., Krummel, M. F. & Allison, J. P. Enhancement of antitumor immunity by
898 CTLA-4 blockade. *Science* **271**, 1734-1736 (1996).
899 https://doi.org:10.1126/science.271.5256.1734
900 7 Hargadon, K. M., Johnson, C. E. & Williams, C. J. Immune checkpoint blockade therapy
901 for cancer: An overview of FDA-approved immune checkpoint inhibitors. *Int*
902 *Immunopharmacol* **62**, 29-39 (2018). https://doi.org:10.1016/j.intimp.2018.06.001
903 8 Wei, S. C., Duffy, C. R. & Allison, J. P. Fundamental Mechanisms of Immune Checkpoint
904 Blockade Therapy. *Cancer Discov* **8**, 1069-1086 (2018). https://doi.org:10.1158/2159-
905 8290.CD-18-0367
906 9 Hodi, F. S. *et al.* Improved survival with ipilimumab in patients with metastatic
907 melanoma. *N Engl J Med* **363**, 711-723 (2010). https://doi.org:10.1056/NEJMoa1003466
908 10 Robert, C. *et al.* Nivolumab in previously untreated melanoma without BRAF mutation.
909 *N Engl J Med* **372**, 320-330 (2015). https://doi.org:10.1056/NEJMoa1412082
910 11 Borghaei, H. *et al.* Nivolumab versus Docetaxel in Advanced Nonsquamous Non-Small-
911 Cell Lung Cancer. *N Engl J Med* **373**, 1627-1639 (2015).
912 https://doi.org:10.1056/NEJMoa1507643
913 12 Brahmer, J. *et al.* Nivolumab versus Docetaxel in Advanced Squamous-Cell Non-Small-
914 Cell Lung Cancer. *N Engl J Med* **373**, 123-135 (2015).
915 https://doi.org:10.1056/NEJMoa1504627
916 13 Motzer, R. J. *et al.* Nivolumab plus Ipilimumab versus Sunitinib in Advanced Renal-Cell
917 Carcinoma. *N Engl J Med* **378**, 1277-1290 (2018).
918 https://doi.org:10.1056/NEJMoa1712126
919 14 Chen, R. *et al.* Phase II Study of the Efficacy and Safety of Pembrolizumab for
920 Relapsed/Refractory Classic Hodgkin Lymphoma. *J Clin Oncol* **35**, 2125-2132 (2017).
921 https://doi.org:10.1200/JCO.2016.72.1316
922 15 El-Khoueiry, A. B. *et al.* Nivolumab in patients with advanced hepatocellular carcinoma
923 (CheckMate 040): an open-label, non-comparative, phase 1/2 dose escalation and
924 expansion trial. *Lancet* **389**, 2492-2502 (2017). https://doi.org:10.1016/S0140-
925 6736(17)31046-2

16 Duffy, A. G. *et al.* Tremelimumab in combination with ablation in patients with advanced hepatocellular carcinoma. *J Hepatol* **66**, 545-551 (2017). https://doi.org:10.1016/j.jhep.2016.10.029

17 Janjigian, Y. Y. *et al.* First-line nivolumab plus chemotherapy versus chemotherapy alone for advanced gastric, gastro-oesophageal junction, and oesophageal adenocarcinoma (CheckMate 649): a randomised, open-label, phase 3 trial. *Lancet* **398**, 27-40 (2021). https://doi.org:10.1016/S0140-6736(21)00797-2

18 Padera, T. P., Meijer, E. F. & Munn, L. L. The Lymphatic System in Disease Processes and Cancer Progression. *Annu Rev Biomed Eng* **18**, 125-158 (2016). https://doi.org:10.1146/annurev-bioeng-112315-031200

19 Zhou, H., Lei, P. J. & Padera, T. P. Progression of Metastasis through Lymphatic System. *Cells* **10** (2021). https://doi.org:10.3390/cells10030627

20 Jones, D. *et al.* Solid stress impairs lymphocyte infiltration into lymph-node metastases. *Nat Biomed Eng* **5**, 1426-1436 (2021). https://doi.org:10.1038/s41551-021-00766-1

21 Lei, P. J. *et al.* Cancer cell plasticity and MHC-II-mediated immune tolerance promote breast cancer metastasis to lymph nodes. *J Exp Med* **220** (2023). https://doi.org:10.1084/jem.20221847

22 Reticker-Flynn, N. E. *et al.* Lymph node colonization induces tumor-immune tolerance to promote distant metastasis. *Cell* **185**, 1924-1942 e1923 (2022). https://doi.org:10.1016/j.cell.2022.04.019

23 Brown, M. *et al.* Lymph node blood vessels provide exit routes for metastatic tumor cell dissemination in mice. *Science* **359**, 1408-1411 (2018). https://doi.org:10.1126/science.aal3662

24 Pereira, E. R. *et al.* Lymph node metastases can invade local blood vessels, exit the node, and colonize distant organs in mice. *Science* **359**, 1403-1407 (2018). https://doi.org:10.1126/science.aal3622

25 Alatengbaolide *et al.* Lymph node ratio is an independent prognostic factor in gastric cancer after curative resection (R0) regardless of the examined number of lymph nodes. *Am J Clin Oncol* **36**, 325-330 (2013). https://doi.org:10.1097/COC.0b013e318246b4e9

26 Aoyama, T. *et al.* The Lymph Node Ratio Is an Independent Prognostic Factor in Pancreatic Cancer Patients Who Receive Curative Resection Followed by Adjuvant Chemotherapy. *Anticancer Res* **38**, 4877-4882 (2018). https://doi.org:10.21873/anticanres.12801

27 Chen, C. C., Lin, J. C. & Chen, K. W. Lymph node ratio as a prognostic factor in head and neck cancer patients. *Radiat Oncol* **10**, 181 (2015). https://doi.org:10.1186/s13014-015-0490-9

28 Scoggins, C. R. *et al.* Prognostic information from sentinel lymph node biopsy in patients with thick melanoma. *Arch Surg* **145**, 622-627 (2010). https://doi.org:10.1001/archsurg.2010.115

29 Voordeckers, M., Vinh-Hung, V., Van de Steene, J., Lamote, J. & Storme, G. The lymph node ratio as prognostic factor in node-positive breast cancer. *Radiother Oncol* **70**, 225-230 (2004). https://doi.org:10.1016/j.radonc.2003.10.015

30 Veronesi, U. *et al.* A randomized comparison of sentinel-node biopsy with routine axillary dissection in breast cancer. *N Engl J Med* **349**, 546-553 (2003). https://doi.org:10.1056/NEJMoa012782

31 Cheng, A. & Lang, J. Survival Analysis of Lymph Node Resection in Ovarian Cancer: A Population-Based Study. *Front Oncol* **10**, 355 (2020). https://doi.org:10.3389/fonc.2020.00355

32 Gortzak-Uzan, L. *et al.* Sentinel lymph node biopsy vs. pelvic lymphadenectomy in early stage cervical cancer: is it time to change the gold standard? *Gynecol Oncol* **116**, 28-32 (2010). https://doi.org:10.1016/j.ygyno.2009.10.049

33 Faries, M. B. *et al.* Completion Dissection or Observation for Sentinel-Node Metastasis in Melanoma. *N Engl J Med* **376**, 2211-2222 (2017). https://doi.org:10.1056/NEJMoa1613210

34 Dammeijer, F. *et al.* The PD-1/PD-L1-Checkpoint Restrains T cell Immunity in Tumor-Draining Lymph Nodes. *Cancer Cell* **38**, 685-700 e688 (2020). https://doi.org:10.1016/j.ccell.2020.09.001

35 Huang, Q. *et al.* The primordial differentiation of tumor-specific memory CD8(+) T cells as bona fide responders to PD-1/PD-L1 blockade in draining lymph nodes. *Cell* (2022). https://doi.org:10.1016/j.cell.2022.09.020

36 Francis, D. M. *et al.* Blockade of immune checkpoints in lymph nodes through locoregional delivery augments cancer immunotherapy. *Sci Transl Med* **12** (2020). https://doi.org:10.1126/scitranslmed.aay3575

37 O'Melia, M. J., Manspeaker, M. P. & Thomas, S. N. Tumor-draining lymph nodes are survival niches that support T cell priming against lymphatic transported tumor antigen and effects of immune checkpoint blockade in TNBC. *Cancer Immunol Immunother* **70**, 2179-2195 (2021). https://doi.org:10.1007/s00262-020-02792-5

38 Eggermont, A. M. *et al.* Adjuvant ipilimumab versus placebo after complete resection of high-risk stage III melanoma (EORTC 18071): a randomised, double-blind, phase 3 trial. *Lancet Oncol* **16**, 522-530 (2015). https://doi.org:10.1016/S1470-2045(15)70122-1

39 van Pul, K. M. *et al.* Local delivery of low-dose anti-CTLA-4 to the melanoma lymphatic basin leads to systemic Treg reduction and effector T cell activation. *Sci Immunol* **7**, eabn8097 (2022). https://doi.org:10.1126/sciimmunol.abn8097

40 Tohme, S., Simmons, R. L. & Tsung, A. Surgery for Cancer: A Trigger for Metastases. *Cancer Res* **77**, 1548-1552 (2017). https://doi.org:10.1158/0008-5472.CAN-16-1536

41 Tang, F., Tie, Y., Tu, C. & Wei, X. Surgical trauma-induced immunosuppression in cancer: Recent advances and the potential therapies. *Clin Transl Med* **10**, 199-223 (2020). https://doi.org:10.1002/ctm2.24

42 Nakajima, Y. *et al.* Near-Infrared Fluorescence Imaging Directly Visualizes Lymphatic Drainage Pathways and Connections between Superficial and Deep Lymphatic Systems in the Mouse Hindlimb. *Sci Rep* **8**, 7078 (2018). https://doi.org:10.1038/s41598-018-25383-y

43 De Togni, P. *et al.* Abnormal development of peripheral lymphoid organs in mice deficient in lymphotoxin. *Science* **264**, 703-707 (1994). https://doi.org:10.1126/science.8171322

1011 44 Mariathasan, S. *et al.* Absence of lymph nodes in lymphotoxin-alpha(LT alpha)-deficient
1012 mice is due to abnormal organ development, not defective lymphocyte migration. *J*
1013 *Inflamm* **45**, 72-78 (1995).
1014 45 Davis, I. A. & Rouse, B. T. Immune responsiveness of lymphotoxin-alpha-deficient mice:
1015 two reconstitution models. *Cell Immunol* **189**, 116-124 (1998).
1016 https://doi.org:10.1006/cimm.1998.1371
1017 46 Banks, T. A. *et al.* Lymphotoxin-alpha-deficient mice. Effects on secondary lymphoid
1018 organ development and humoral immune responsiveness. *J Immunol* **155**, 1685-1693
1019 (1995).
1020 47 Meijer, E. F. J. *et al.* Lymph node effective vascular permeability and chemotherapy
1021 uptake. *Microcirculation* **24** (2017). https://doi.org:10.1111/micc.12381
1022 48 Suami, H. *et al.* A new indocyanine green fluorescence lymphography protocol for
1023 diagnostic assessment of lower limb lymphoedema. *J Plast Reconstr Aesthet Surg*
1024 (2022). https://doi.org:10.1016/j.bjps.2022.08.017
1025 49 Maaskant-Braat, A. J. *et al.* Lymphatic mapping after previous breast surgery. *Breast* **21**,
1026 444-448 (2012). https://doi.org:10.1016/j.breast.2011.10.007
1027 50 Sato, A. *et al.* Altered lymphatic drainage patterns in re-operative sentinel lymph node
1028 biopsy for ipsilateral breast tumor recurrence. *Radiat Oncol* **14**, 159 (2019).
1029 https://doi.org:10.1186/s13014-019-1367-0
1030 51 Bronte, V. & Pittet, M. J. The spleen in local and systemic regulation of immunity.
1031 *Immunity* **39**, 806-818 (2013). https://doi.org:10.1016/j.immuni.2013.10.010
1032 52 Tomura, M. *et al.* Monitoring cellular movement in vivo with photoconvertible
1033 fluorescence protein "Kaede" transgenic mice. *Proc Natl Acad Sci U S A* **105**, 10871-
1034 10876 (2008). https://doi.org:10.1073/pnas.0802278105
1035 53 Helft, J. *et al.* GM-CSF Mouse Bone Marrow Cultures Comprise a Heterogeneous
1036 Population of CD11c(+)MHCII(+) Macrophages and Dendritic Cells. *Immunity* **42**, 1197-
1037 1211 (2015). https://doi.org:10.1016/j.immuni.2015.05.018
1038 54 Wolchok, J. D. *et al.* Long-Term Outcomes With Nivolumab Plus Ipilimumab or
1039 Nivolumab Alone Versus Ipilimumab in Patients With Advanced Melanoma. *J Clin Oncol*
1040 **40**, 127-137 (2022). https://doi.org:10.1200/JCO.21.02229
1041 55 Siddiqui, I. *et al.* Intratumoral Tcf1(+)PD-1(+)CD8(+) T Cells with Stem-like Properties
1042 Promote Tumor Control in Response to Vaccination and Checkpoint Blockade
1043 Immunotherapy. *Immunity* **50**, 195-211 e110 (2019).
1044 https://doi.org:10.1016/j.immuni.2018.12.021
1045 56 Paz-Ares, L. *et al.* Pembrolizumab plus Chemotherapy for Squamous Non-Small-Cell Lung
1046 Cancer. *N Engl J Med* **379**, 2040-2051 (2018). https://doi.org:10.1056/NEJMoa1810865
1047 57 Reck, M. *et al.* Pembrolizumab versus Chemotherapy for PD-L1-Positive Non-Small-Cell
1048 Lung Cancer. *N Engl J Med* **375**, 1823-1833 (2016).
1049 https://doi.org:10.1056/NEJMoa1606774
1050 58 Swoboda, A. & Nanda, R. Immune Checkpoint Blockade for Breast Cancer. *Cancer Treat*
1051 *Res* **173**, 155-165 (2018). https://doi.org:10.1007/978-3-319-70197-4_10
1052 59 Weber, J. *et al.* Adjuvant Nivolumab versus Ipilimumab in Resected Stage III or IV
1053 Melanoma. *N Engl J Med* **377**, 1824-1835 (2017).
1054 https://doi.org:10.1056/NEJMoa1709030

1055 60 Weber, J. S. *et al.* Adjuvant Therapy of Nivolumab Combined With Ipilimumab Versus
1056 Nivolumab Alone in Patients With Resected Stage IIIB-D or Stage IV Melanoma
1057 (CheckMate 915). *J Clin Oncol*, JCO2200533 (2022).
1058 https://doi.org:10.1200/JCO.22.00533
1059 61 Patel, S. P. *et al.* Neoadjuvant-Adjuvant or Adjuvant-Only Pembrolizumab in Advanced
1060 Melanoma. *N Engl J Med* **388**, 813-823 (2023). https://doi.org:10.1056/NEJMoa2211437
1061 62 Lo, J. A. *et al.* Epitope spreading toward wild-type melanocyte-lineage antigens rescues
1062 suboptimal immune checkpoint blockade responses. *Sci Transl Med* **13** (2021).
1063 https://doi.org:10.1126/scitranslmed.abd8636
1064 63 Baeyens, A., Fang, V., Chen, C. & Schwab, S. R. Exit Strategies: S1P Signaling and T Cell
1065 Migration. *Trends Immunol* **36**, 778-787 (2015). https://doi.org:10.1016/j.it.2015.10.005
1066 64 Cyster, J. G. & Schwab, S. R. Sphingosine-1-phosphate and lymphocyte egress from
1067 lymphoid organs. *Annu Rev Immunol* **30**, 69-94 (2012). https://doi.org:10.1146/annurev-
1068 immunol-020711-075011
1069 65 Girard, J. P., Moussion, C. & Forster, R. HEVs, lymphatics and homeostatic immune cell
1070 trafficking in lymph nodes. *Nat Rev Immunol* **12**, 762-773 (2012).
1071 https://doi.org:10.1038/nri3298
1072 66 Brinkmann, V., Cyster, J. G. & Hla, T. FTY720: sphingosine 1-phosphate receptor-1 in the
1073 control of lymphocyte egress and endothelial barrier function. *Am J Transplant* **4**, 1019-
1074 1025 (2004). https://doi.org:10.1111/j.1600-6143.2004.00476.x
1075 67 Borsetto, D. *et al.* The risk of recurrence in surgically treated head and neck squamous
1076 cell carcinomas: a conditional probability approach. *Acta Oncol* **60**, 942-947 (2021).
1077 https://doi.org:10.1080/0284186X.2021.1925343
1078 68 Darragh, L. B. *et al.* A phase I/Ib trial and biological correlate analysis of neoadjuvant
1079 SBRT with single-dose durvalumab in HPV-unrelated locally advanced HNSCC. *Nat*
1080 *Cancer* **3**, 1300-1317 (2022). https://doi.org:10.1038/s43018-022-00450-6
1081 69 Saddawi-Konefka, R. *et al.* Lymphatic-preserving treatment sequencing with immune
1082 checkpoint inhibition unleashes cDC1-dependent antitumor immunity in HNSCC. *Nat*
1083 *Commun* **13**, 4298 (2022). https://doi.org:10.1038/s41467-022-31941-w
1084 70 Ascierto, P. A. *et al.* Adjuvant nivolumab versus ipilimumab in resected stage IIIB-C and
1085 stage IV melanoma (CheckMate 238): 4-year results from a multicentre, double-blind,
1086 randomised, controlled, phase 3 trial. *Lancet Oncol* **21**, 1465-1477 (2020).
1087 https://doi.org:10.1016/S1470-2045(20)30494-0
1088 71 Haley, P. J. The lymphoid system: a review of species differences. *J Toxicol Pathol* **30**,
1089 111-123 (2017). https://doi.org:10.1293/tox.2016-0075
1090 72 Fu, C. & Jiang, A. Dendritic Cells and CD8 T Cell Immunity in Tumor Microenvironment.
1091 *Front Immunol* **9**, 3059 (2018). https://doi.org:10.3389/fimmu.2018.03059
1092 73 Bery, A. I. *et al.* Role of tertiary lymphoid organs in the regulation of immune responses
1093 in the periphery. *Cellular and molecular life sciences : CMLS* **79**, 359 (2022).
1094 https://doi.org:10.1007/s00018-022-04388-x
1095 74 Wijeyesinghe, S. *et al.* Expansible residence decentralizes immune homeostasis. *Nature*
1096 **592**, 457-462 (2021). https://doi.org:10.1038/s41586-021-03351-3

1097 75 Janneh, A. H. *et al.* Crosstalk between pro-survival sphingolipid metabolism and
1098 complement signaling induces inflammasome-mediated tumor metastasis. *Cell Rep* **41**,
1099 111742 (2022). https://doi.org:10.1016/j.celrep.2022.111742
1100 76 Shi, W. *et al.* SphK2/S1P Promotes Metastasis of Triple-Negative Breast Cancer Through
1101 the PAK1/LIMK1/Cofilin1 Signaling Pathway. *Front Mol Biosci* **8**, 598218 (2021).
1102 https://doi.org:10.3389/fmolb.2021.598218
1103 77 Perlman, R. L. Mouse models of human disease: An evolutionary perspective. *Evol Med*
1104 *Public Health* **2016**, 170-176 (2016). https://doi.org:10.1093/emph/eow014
1105 78 Heydon-White, A., Suami, H., Boyages, J., Koelmeyer, L. & Peebles, K. C. Assessing breast
1106 lymphoedema following breast cancer treatment using indocyanine green
1107 lymphography. *Breast Cancer Res Treat* **181**, 635-644 (2020).
1108 https://doi.org:10.1007/s10549-020-05661-y
1109 79 Onoi, K. *et al.* Immune Checkpoint Inhibitors for Lung Cancer Treatment: A Review. *J Clin*
1110 *Med* **9** (2020). https://doi.org:10.3390/jcm9051362
1111 80 Boukouris, A. E. *et al.* Latest evidence on immune checkpoint inhibitors in metastatic
1112 colorectal cancer: A 2022 update. *Crit Rev Oncol Hematol* **173**, 103663 (2022).
1113 https://doi.org:10.1016/j.critrevonc.2022.103663
1114 81 Barreto de Albuquerque, J. *et al.* Microbial uptake in oral mucosa-draining lymph nodes
1115 leads to rapid release of cytotoxic CD8(+) T cells lacking a gut-homing phenotype. *Sci*
1116 *Immunol* **7**, eabf1861 (2022). https://doi.org:10.1126/sciimmunol.abf1861
1117 82 Li, A. & Bergan, R. C. Clinical trial design: Past, present, and future in the context of big
1118 data and precision medicine. *Cancer* **126**, 4838-4846 (2020).
1119 https://doi.org:10.1002/cncr.33205
1120 83 Jones, D., Pereira, E. R. & Padera, T. P. Growth and Immune Evasion of Lymph Node
1121 Metastasis. *Front Oncol* **8**, 36 (2018). https://doi.org:10.3389/fonc.2018.00036
1122 84 Rahim, M. K. *et al.* Dynamic CD8(+) T cell responses to cancer immunotherapy in human
1123 regional lymph nodes are disrupted in metastatic lymph nodes. *Cell* **186**, 1127-1143
1124 e1118 (2023). https://doi.org:10.1016/j.cell.2023.02.021
1125 85 Wurdinger, T. *et al.* A secreted luciferase for ex vivo monitoring of in vivo processes. *Nat*
1126 *Methods* **5**, 171-173 (2008). https://doi.org:10.1038/nmeth.1177
1127 86 CoreTeam, R. R: A language and environment for statistical computing. *R Foundation for*
1128 *Statistical Computing, Vienna, Austria.* (2021).
1129